

STATISTICAL TESTS FOR REPLACING HUMAN DECISION MAKERS WITH ALGORITHMS

Kai Feng¹, Han Hong², Ke Tang¹, and Jingyuan Wang³

¹Institute of Economics, School of Social Sciences, Tsinghua University,

Email: fengk22@mails.tsinghua.edu.cn, ketang@tsinghua.edu.cn

²Department of Economics, Stanford University, Email: doubleh@stanford.edu

³School of Economics and Management, Beihang University, Email: jyyang@buaa.edu.cn

December 10, 2024

ABSTRACT. This paper proposes a statistical framework of using artificial intelligence to improve human decision making. The performance of each human decision maker is benchmarked against that of machine predictions. We replace the diagnoses made by a subset of the decision makers with the recommendation from the machine learning algorithm. We apply both a heuristic frequentist approach and a Bayesian posterior loss function approach to abnormal birth detection using a nationwide dataset of doctor diagnoses from pregnancy checkups of reproductive age couples and pregnancy outcomes. We find that our algorithm on a test dataset results in a higher overall true positive rate and a lower false positive rate than the diagnoses made by doctors only.

KEYWORDS: Artificial Intelligence, Machine Learning, Decision Making, ROC Curve

JEL Classification: C44, C11, C12

1 Introduction

In the current era of machine learning, artificial intelligence (AI) algorithms have emerged as valuable tools that can learn significant features from data and potentially facilitate decision making in various disciplines. In medical research, [Esteva et al. \(2017\)](#) and [Kermany et al. \(2018\)](#) utilize deep neural network to automate diagnosis based on medical images. [Berg et al. \(2020\)](#) and [Sadhvani et al. \(2021\)](#) leverage machine learning algorithms to predict the default probability for bank lending decision. [Mullainathan and Spiess \(2017\)](#) and [Athey and Imbens \(2019\)](#) apply machine learning models to broad optimal policy assignment problems.

A considerable number of papers have compared the performance of algorithms with that of the representative human decision makers. To mention a few, [Esteva et al. \(2017\)](#) claims that their algorithm outperformed the aggregate dermatologist on some skin cancer classification tasks; [Kermany et al. \(2018\)](#) targets macular degeneration diagnosis and concluded that the machine algorithm outperforms some retinologists; [Rajpurkar et al. \(2017\)](#) highlights the performance gain of a deep convolutional neural network over an aggregate cardiologist for processing ECG sequences; [Kleinberg et al. \(2018\)](#) trains a gradient boosted decision tree model to predict crime risk during pre-trial bail and suggested that substituting human judges with the algorithm could result in large welfare gains.

The findings of the aforementioned literature rely mostly on the observation that the pair of false positive rate (FPR) and true positive rate (TPR) point lies strictly below the receiver operating characteristic (ROC) curve generated by the machine learning algorithm, implying that algorithms can achieve a higher TPR for a given FPR or a lower FPR for a given TPR. In binary classification / decision making, FPR is the number of wrongly classified negative events divided by the number of actual negative events, and TPR is the number of correctly classified positive events divided by the number of total positive events. FPR/TPR are synonymous to size and power in classical hypothesis testing.

We first *caution against* such interpretations without a deeper understanding of human decision making processes. The literature findings can be rationalized not only by the superior information quality of algorithms but also by the *incentive heterogeneity*, i.e. the differential preferences for taking the same action by multiple human decision makers, some of whom can be no less accurate than algorithms in processing information from observational data. Machine algorithms provide information, but decision making is a combination of incentives and information. Using machine algorithms to assist with decision making necessitates the modeling of incentives. Second, the FPR/TPR pairs of human decision makers are typically *imprecisely measured*, especially when the number of cases for each decision makers is not large. The data in our empirical analysis shows not only substantial heterogeneity between individual doctors, but also that the randomness in measuring the quality of decision makers plays a key role when the performance of decision makers is compared to that of machine algorithms.

To illustrate the first issue of concern, consider Figure 1, in which a collection of FPR/TPR pairs for human decision makers, denoted as $j = 1, \dots, J$, all lie approximately on a ROC curve generated by their employed decision rules $\hat{Y}_{i,j} = \mathbb{1}(p(X_{i,j}, U_{i,j}) > c_j)$ with different individual cutoff threshold c_j for decision maker j . In the decision rule, $X_{i,j}$ are observed features used in the machine learning algorithm; $U_{i,j}$ are private information only observable to the human decision makers, and $p(x, u) = \mathbb{P}(Y = 1|x, u)$ is a propensity score function. Also drawn is the machine ROC curve based on classification rules $\hat{Y}_i = \mathbb{1}(p(X_i) > c)$, which collects the corresponding FPR/TPR pairs by varying the cutoff threshold c , and where $p(x) = \mathbb{P}(Y = 1|x)$ is the correctly specified propensity score function using observable features x discovered by the machine learning algorithm. However, after averaging over all decision makers, the aggregate human FPR/TPR point lies visibly below the machine ROC curve.

[Figure 1 about here.]

Our paper makes several contributions. First, we offer a conceptual framework of information and incentives for interpreting comparisons between the machine algorithms and human decision makers. Second, we provide a model to identify human decision maker candidates for replacement by machine algorithms and to generate machine algorithm based decisions that incorporate human decision maker preferences. The replacement model accounts for the sampling uncertainty of individual decision makers. Third, an empirical application to abnormal birth detection demonstrates that our proposed replacement algorithm significantly improves the overall performance of risky pregnancy detection. Fourth, we conduct an extensive synthetic data analysis that serves as guidance for evaluating empirical procedures incorporating complementarity in the presence of information asymmetry between human decision maker and machine algorithms.

In this paper, in order to compare machines with human decision makers, we restrict incentive heterogeneity and focus on information processing capacity. If the individual FPR/TPR pairs are precisely known without sampling errors, they can be directly compared to the machine ROC curve; we interpret a human FPR/TPR pair below the machine ROC curve as evidence of the superiority of the machine algorithms. As shown in Figure 2, a human FPR/TPR pair below the machine ROC curve can be dominated by any point on the line segment of the ROC curve between A and B. Replacing the human FPR/TPR pair by any point on the A-B segment of the machine ROC curve segment results in higher TPR without increasing FPR, or lower FPR without sacrificing TPR.

In reality, only an *estimate* of the FPR/TPR pair can be obtained from the empirical data. A statistical framework to compare the performance of algorithms with that of human decision makers requires accounting for estimation sampling errors. We focus on two main issues. First, we seek statistical evidence supporting the information superiority of an algorithm that favors the replacement of a human decision maker. Second, we aim to identify the most

appropriate point on the machine ROC curve for this purpose. To address these two issues, we experiment with both a heuristic frequentist confidence set approach and a subsequent Bayesian inference approach. In both scenarios, confidence and credible regions are formed to inform the decision making process. The Bayesian approach results in more replacement and additional improvement in the aggregate FPR/TPR pair. We suggest the Bayesian analysis as an applicable decision framework.

At a disaggregated level, each individual human can have either less or more information processing capacity than an algorithm has. For instance, [Liang et al. \(2019\)](#) proposes a machine learning algorithm to diagnose childhood diseases that outperforms junior physician groups but marginally underperforms senior physician groups. Similar findings are reported in [Peng et al. \(2021\)](#). [Esteva et al. \(2017\)](#) and [Kermany et al. \(2018\)](#) also find substantial variability in the human experts' performance. Our framework chooses between each human decision maker and the algorithm for making future decisions. We identify a subset of human decision makers to be replaced by the algorithm, whereas the rest of human decision makers are retained.

We apply our statistical framework to a unique National Free Prepregnancy Checkups (NFPC) dataset. The NFPC is a free health checkup service for conceiving couples across 31 provinces in China. In addition to the pregnancy outcome and numerous patient-case features, the dataset also includes the doctors' IDs and diagnoses of adverse pregnancy outcomes. We first split the data into two parts. The first part is used to compare doctors with algorithms. Specifically, we employ a random forest (RF) method for diagnosing risky pregnancy, which achieves an area under the curve (AUC) above 0.68. Using 95% credible level, our Bayesian approach suggests that the random forest algorithm outperforms 46.1% of doctors. The second part of the dataset is used to evaluate the quality of the diagnosis procedure based on the combination of retained doctors and the algorithm. The combined decision making procedure achieves an increase of 46.6% in the TPR and a reduction of 10.1% in the FPR. Additional detailed analysis further shows that the potential for machine algorithms to improve decision making quality is substantial even when only a smaller portion of doctors are replaced. We also find that doctors practicing only in country hospitals have a lower replacement ratio compared with those having practiced in township clinics. The result of our Bayesian analysis suggests that 51.2% of doctors who have practiced only at township clinics are replaced compared to 39.8% of doctors who have practiced only at county hospitals.

Related Literature Our paper relates to several strands of literature. An extensive literature studies the utilization of AI to enhance medical diagnostic capabilities. Machine learning, especially deep learning methods, which demonstrate great potential in tackling diverse and complex tasks, has been experimented to diagnose in multiple medical subfields, including ophthalmology ([Kermany et al., 2018](#)); cardiology ([Rajpurkar et al., 2017](#); [Hannun et al., 2019](#)); dermatology ([Esteva et al., 2017](#)); respirology ([Ardila et al., 2019](#); [Liang et al., 2019](#)); clinical

psychology and psychiatry (Ashar et al., 2017; Yoon et al., 2022); tumor and cancer detection (McKinney et al., 2020; Peng et al., 2021; Uhm et al., 2021; Tian et al., 2024). Additional surveys can be found in Erickson et al. (2017), Johnson et al. (2018), Dwyer et al. (2018), Chan et al. (2020), Huang et al. (2020) and Swanson et al. (2023).

Beyond medical diagnoses, AI is widely explored in social-economic decision making. See for example Berg et al. (2020), Sadhwani et al. (2021) and Fekadu et al. (2022) for loan approval and credit risk modeling; Fuster et al. (2019), Vallee and Zeng (2019) and Fuster et al. (2022) for market structure implications of employing machine learning algorithms; Berk (2017), Zeng et al. (2017), Kleinberg et al. (2018) for bail and parole analysis; Chalfin et al. (2016) and Sajjadiyani et al. (2019) for productivity assessment.

Numerous papers in the literature have benchmark algorithms against human decision makers¹. While machine algorithms often outperform some aggregation of human decision makers, these findings are not uniform across individual human decision makers. Unlike machine algorithms, human decision makers can be highly heterogeneous in both incentives and information processing capacity. The health economics literature suggests that doctors may be swayed by multiple non-medical incentives including lawsuit avoidance (Studdert et al., 2005), financial gain (Johnson and Rehavi, 2016), demand pressure from patient (Lopez et al., 2018) and procedural skills (Currie and MacLeod, 2017). Our analysis highlights the importance of modeling and restricting incentive heterogeneity in a human-AI comparison.

A growing literature also explores AI assisted human decision making. While Brennan et al. (2019), Han et al. (2020), Peng et al. (2021), Yang et al. (2021) and Tian et al. (2024) report salient performance improvement when doctors can refer to the prediction results of algorithms, Jin et al. (2024) and Yu et al. (2024) report contradicting evidence where the performance of a portion of doctors is worsened by AI assistance. By offering doctors monetary incentives prior to the experiment, Wang et al. (2023) and Wang et al. (2024) find that doctor diagnoses can be significantly influenced by both the machine information and the preset incentive structures. While both Bansal et al. (2021) and Wang et al. (2023) find that giving doctors explanations increases the acceptance of machine recommendations, the effect of providing explanation on performance is inconclusive and varies. In the beverage vending machine business, a field experiment on product assortment decision conducted by Kawaguchi (2021) finds heterogeneous adoption by workers dependent on location and both worker and machine characteristics. Alur et al. (2023) propose a test whether human experts help improve machine algorithm predictions. Our analysis also suggests that the human machine complementarity, argued for by Donahue et al. (2022), is not only theoretically challenging but also difficult to implement empirically. Overall, the mechanism by which AI assists human decision making is unclear. Our paper

¹See for example Long et al. (2017), Kermany et al. (2018), De Fauw et al. (2018), Rajpurkar et al. (2017), Hannun et al. (2019), Esteva et al. (2017), Han et al. (2020), Daneshjou et al. (2022), Ardila et al. (2019), Liang et al. (2019), McKinney et al. (2020), Peng et al. (2021), Uhm et al. (2021), Tian et al. (2024), Berk (2017), Kleinberg et al. (2018), Han et al. (2020).

thus focuses on a simple strategy that identifies and replaces underperforming doctors. This modeling choice is also consistent with the analysis in [Mullainathan and Obermeyer \(2022\)](#) and [Chan et al. \(2022\)](#) who suggest that doctor performance can not be explained by preference heterogeneity alone. In addition, the case-specific replacement algorithm described in [Appendix A.6](#) does not outperform the baseline method for our NFPC dataset.

A substantial body of literature discusses the discriminatory bias of algorithms ([O’neil, 2017](#); [Eubanks, 2018](#); [Berk et al., 2021](#)). But the potential of AI and algorithmic decision making to reverse extant bias in the training data is also noted by [Rambachan and Roth \(2019\)](#) and [Rambachan et al. \(2020\)](#). Through efficient information provision and scarce resource utilization, AI can be instrumental for inequality reduction. Using artificial intelligence to empower medical diagnose in developing areas has been advocated by researches including [Adepoju et al. \(2017\)](#); [Guo and Li \(2018\)](#); [Trivedi et al. \(2019\)](#); [Mondal et al. \(2023\)](#) and others. [Bulathwela et al. \(2021\)](#) discuss the comprehensive application of AI to narrow education inequality gap. Our finding using the NFPC dataset is also consistent with anecdotal information regarding the quality disparity across tiers of the hospital classification system in China.

Optimal decision making using machine learning techniques is also drawing increasing attention from econometrics. [Kitagawa and Tetenov \(2018\)](#), [Mbakop and Tabord-Meehan \(2021\)](#), [Athey and Wager \(2021\)](#) and [Feng and Hong \(2024\)](#) explore the asymptotic properties of empirical algorithm based optimal decision making. [Manski \(2018\)](#) considers the identification problem when only the prediction conditional on a subset of covariates and the conditional distribution of the “omitted” covariates are known. In this paper, we assume, as in the baseline cases of [Kitagawa and Tetenov \(2018\)](#), that the machine algorithm is known and deterministic, in view of the large data size and the comprehensive list of covariates in the NFPC dataset.

The rest of this paper is organized as follows. [Section 2](#) presents the statistical model of human-algorithm comparison. [Section 3](#) describes the data and the algorithm. [Section 4](#) reports results from the empirical analysis of the machine algorithm and human decision makers. [Section 5](#) presents a set of synthetic data analysis for additional insights, and [Section 6](#) concludes. Additional results are collected in the [Appendix](#).

2 Replacing Human Decision Makers with Algorithms

Consider a sample dataset with labels $Y_i \in \{0, 1\}$ and features $X_i, i = 1, \dots, n$. Define

$$\text{TPR} = \frac{\frac{1}{n} \sum_{i=1}^n Y_i \hat{Y}_i}{\hat{p}}, \quad \text{FPR} = \frac{\frac{1}{n} \sum_{i=1}^n (1 - Y_i) \hat{Y}_i}{1 - \hat{p}}, \quad \hat{p} = \frac{1}{n} \sum_{i=1}^n \hat{Y}_i, \quad (1)$$

where $\hat{Y}_i \in \{0, 1\}$ is a predictor for Y_i based on a general decision rule, such that (X_i, Y_i, \hat{Y}_i) are i.i.d draws from an underlying population. The Law of Large Number implies that the

FPR/TPR converge to their population analogs (denoted as β and α) as $n \rightarrow \infty$:

$$\beta = \frac{1}{p} \mathbb{E} Y_i \hat{Y}_i, \quad \alpha = \frac{1}{1-p} \mathbb{E} \left[(1 - Y_i) \hat{Y}_i \right], \quad \text{where } p = \mathbb{E} Y_i = \mathbb{P}(Y_i = 1). \quad (2)$$

A key concept in this paper is *incentive heterogeneity*. In general terms, incentive refers to the motivation of certain actions, and incentive heterogeneity refers to different payoffs across multiple human decision makers for taking the same actions. Incentive heterogeneity can typically be classified intuitively as either intra-individual or inter-individual. On the one hand, inter-individual incentive heterogeneity refers to situations where the cost assessment only varies across decision makers but not across individual cases for each decision maker. On the other hand, intra-individual incentive heterogeneity refers to situations where the cost assessments across individual cases for a given decision maker vary based on both publicly observed features x that are accessible by the machine algorithm and private information features u that are only available to human decision makers. To compare human decision makers and machines, we make the following two assumptions regarding incentive heterogeneity:

Assumption 1. *The machine ROC curve is generated by a propensity score model of prediction:*

$$\hat{y}_{i,M} = \mathbf{1}(m(x_i) > c).$$

The decision maker j 's decision is also based on a perceived propensity score model:

$$\hat{y}_{i,j} = \mathbf{1}(q_j(x_{i,j}, u_{i,j}) > c_j).$$

Both $m(\cdot)$ and $q_j(\cdot)$ can be correctly specified or misspecified.

Assumption 1 rules out intra-individual incentive heterogeneity and allows us to focus on inter-individual incentive heterogeneity. Doctors in our dataset exhibit highly variable degrees of conservativeness in their diagnoses. The FPR of the doctors with at least 300 diagnoses has a mean of 0.236 and a standard deviation of 0.230. Some doctors tend to diagnose almost all patients as highly risky, and some doctors rarely make a positive diagnosis. Figure 5 illustrates. The diffusive distribution of doctors' FPR/TPR pairs also indicates both information processing capacity difference and inter-individual heterogeneity. The analysis in Chan et al. (2022) shows that when only either diagnostic skill difference or inter-individual incentive heterogeneity is present, the doctors FPR/TPR pairs will concentrate in a small region, which is not the case in Figure 5. Importantly, Assumption 1 also allows for private information $u_{i,j}$ that is only observed by the doctors and not used in the machine learning algorithm. In the absence of the private information variable $u_{i,j}$, the doctors' diagnoses are perfectly predictable by the machine learning algorithm, which is very unlikely.

Assumption 2. *The machine propensity score model $m(x_i)$ and the j th decision maker’s propensity score model $q_j(x_{i,j}, u_{i,j})$ are used without sampling errors in the machine decision making procedure and by the j th decision maker, respectively.*

The first requirement is justified by the fact that the machine learning model is implemented using a training dataset that is by orders of magnitude larger than the number of cases for each individual human decision maker. For instance, around 150 thousand cases in the NFPC training dataset are used to estimate the machine ROC curve, whereas the median number of diagnoses per doctor in the classification set is only approximately 400. The estimation error in the machine ROC curve is negligible relative to the error in estimating doctors’ FPR/TPR pairs. The sampling error in estimating the machine ROC curve is studied in a subsequent paper by [Feng and Hong \(2024\)](#).

The second requirement that the $q_j(x_{i,j}, u_{i,j})$ are used without sampling errors by the j th decision maker is interpreted as stating that the behavior of the j th decision maker is consistent with the use of a propensity score model $q_j(x_{i,j}, u_{i,j})$. The method in this paper does not require the researcher to know the propensity score model $q_j(x_{i,j}, u_{i,j})$ for the j th decision maker, and does not refer to any of the doctor propensity score models $q_j(x_{i,j}, u_{i,j}), j = 1, \dots, J$. The second requirement also rules out decision makers learning from the sample cases. A doctor j does not update their propensity score model $q_j(x_{i,j}, u_{i,j})$ during the data sample period.

This is a reasonable assumption in our empirical dataset because the eventual pregnancy outcomes are typically not available to doctors when they diagnose consecutive patient cases. We are not concerned with how doctors procure knowledge to develop their diagnosis model $q_j(x_{i,j}, u_{i,j})$. Doctor j might procure $q_j(x_{i,j}, u_{i,j})$ from trainings obtained from a medical school or from working with a large pool of patients prior to the sampling period. [Section 3](#) provides more details about the data processing procedure, where sampling errors arise mainly from the relatively fewer number of observations for each individual decision maker.

2.1 Human FPR/TPR pairs and ROC curves in the population

The parameter of interest is the population pair of true positive and false positive rates for an individual decision maker: $\theta_H = (\alpha_H, \beta_H)$, where α and β are defined as in [\(2\)](#) and the subscript H refers to “human”. If θ_H is above a machine ROC curve, as in [Figure 1](#), then given the FPR α_H , the algorithm has a lower TPR β_M than humans have. Similarly, given the TPR β_H , the machine has a larger FPR α_M than humans have. In this sense, humans outperform the algorithm. In particular, under [Assumption 1](#), if humans correctly use at least as much information as the algorithm does, in the sense that the propensity model is correctly specified, then θ_H lies above the machine ROC. The formal argument is given in [Lemma A.1](#) in the appendix.

[Figure 2](#) shows a θ_H pair for a human decision maker that is below the machine ROC curve.

A machine decision rule corresponding to a point on the machine ROC curve between A and B performs better than the human decision maker. The segment of the curve to the left of B (to the right of A) has a smaller α_M but a smaller β_M (a larger β_M but a larger α_M) than the human decision maker. These segments of the machine ROC curve are not directly comparable to the human decision maker.

[Figure 2 about here.]

The classical Neyman-Pearson lemma states that when $p(x) = \mathbb{P}(Y = 1|x)$ is correctly specified, for any pair of positive numbers (η, ϕ) , there exists a cutoff value c , such that the point (α_c, β_c) on the ROC curve corresponding to the decision rule $\hat{y} = \mathbb{1}(p(x) > c)$ maximizes a linear combination $\phi\beta - \eta\alpha$ of the TPR and FPR. Conversely, each point on this ROC curve optimizes some linear combination of TPR and FPR. Neyman-Pearson Lemma is also motivated by a Bayesian decision maker who minimizes posterior expected loss of misclassification upon observing the features x , based on a loss matrix of the following form:

$$\begin{array}{rcc} \text{Loss matrix} & \hat{y} = 0 & \hat{y} = 1 \\ y = 0 & 0 & c_{01} \\ y = 1 & c_{10} & 0, \end{array}$$

where c_{10} represents the cost of misclassifying 1 as 0 and c_{01} represents the cost of misclassifying 0 as 1. Each point on the ROC curve, corresponding to a decision rule $\hat{y} = \mathbb{1}(p(x) > c)$, minimizes Bayesian posterior expected loss for some choice of c_{10} and c_{01} through the relation $c = \frac{c_{01}}{c_{10} + c_{01}}$. Importantly, the cost matrix c_{01}, c_{10} and linear combination coefficients η, ϕ in the Neyman-Pearson Lemma are independent of the features x in order to provide optimality justification of the points on the ROC curve. Assumption 1 is then interpreted as each doctor behaving as a Bayesian decision maker adopting the same constant cost matrix c_{10} and c_{01} among their patients. The ex ante expected minimized cost for the Bayesian decision maker corresponds to a linear combination of FPR and TPR:

$$c_{10}\mathbb{E}\left[p(X)(1 - \hat{Y})\right] + c_{01}\mathbb{E}\left[(1 - p(X))\hat{Y}\right] = (1 - p)c_{01}\text{FPR} - pc_{10}\text{TPR} + pc_{10}.$$

If we denote point A and B in Figure 2 as (α_H, β_R) and (α_R, β_H) , then any point (α_M, β_M) between (α_R, β_H) and (α_H, β_R) on the machine ROC curve satisfies $\alpha_M < \alpha_H$ and $\beta_M > \beta_H$. For arbitrary $\phi, \eta > 0$ and c_{10}, c_{01} ,

$$\begin{aligned} \eta\alpha_M - \phi\beta_M &< \eta\alpha_H - \phi\beta_H, \quad \text{and} \\ (1 - p)c_{01}\alpha_M - pc_{10}\beta_M &< (1 - p)c_{01}\alpha_H - pc_{10}\beta_H. \end{aligned}$$

Therefore, compared with human decisions, any point (α_M, β_M) between (α_R, β_H) and (α_H, β_R) on the ROC curve achieves a better linear combination for all possible values of ϕ, η , and lower expected cost for all loss matrixes of c_{01}, c_{10} . In this sense, (α_M, β_M) *dominates* (α_H, β_H) .

Recall that θ_H is a population parameter that measures the expected performance of the human decision maker. When θ_H lies below the machine ROC curve, *on average*, the machine algorithm can outperform the human decision maker by increasing the population TPR or reducing the population FPR. However, unless the algorithm can make predictions with perfect accuracy, for each specific patient case, the human decision maker can either underperform or outperform the algorithm.

Our framework is likely to be applicable when people make many repeated decisions to allow for a sufficiently precise estimate of their error rates. It is less applicable in situations when people only ever make a few decisions of a type, a setting that may arise even when decisions are frequent if some action rarely is or should be taken. The lack of information renders the task of distinguishing humans from algorithms difficult, even if humans might be detectably worse in aggregate². Our application features a comprehensive set of covariates, a large dataset, reliable and measurable outcomes, and a stable prediction environment that are consistent with the scenarios in the important papers by [Kahneman and Klein \(2009\)](#) and [Currie and MacLeod \(2017\)](#).

2.2 Human FPR/TPR pair and ROC curve comparison in the sample

Typically, the population value of θ_H is not directly observed, and instead needs to be estimated from a dataset. Denote the the sample estimates (FPR, TPR) in (1) as $\hat{\theta}_H = (\hat{\alpha}_H, \hat{\beta}_H)$. In the presence of sampling uncertainty, the inference problem pertains to how we can make a probabilistic statement regarding whether θ_H is above or below the machine ROC curve. From a frequentist analysis point of view, because the sample estimate $\hat{\theta}_H$ is a vector function of a multinomial distribution, the finite sample distribution function of $\hat{\theta}_H$ can be analytically intractable. Large sample frequentist analysis and simulation methods, however, are facilitated by the joint asymptotic normal distribution of $\hat{\theta}_H$.

Lemma 2.1. *For an i.i.d. sample $\{Y_i, \hat{Y}_i\}_i^n$, the joint asymptotic distribution of a human FPR/TPR pair $\hat{\theta}_H = (\hat{\alpha}_H, \hat{\beta}_H)$ is multivariate normal. In particular*

$$\sqrt{n} \left(\hat{\theta}_H - \theta_H \right) \xrightarrow{d} N(0, \Sigma), \quad \Sigma = \begin{pmatrix} \frac{\alpha_H(1-\alpha_H)}{1-p} & 0 \\ 0 & \frac{\beta_H(1-\beta_H)}{p} \end{pmatrix}.$$

The proof of Lemma 2.1 is given in the appendix and follows from standard arguments for approximating multinomial distributions with normal limits. The asymptotic covariance Σ can be consistently estimated by a sample analog $\hat{\Sigma}$ where the parameters α_H, β_H and p are replaced by $\hat{\alpha}_H, \hat{\beta}_H$ and \hat{p} . The resulting asymptotic confidence set of the FPR/TPR pairs is elliptically

²We are grateful to the associate editor for pointing out this important clarification.

shaped. As illustrated in Figure 3(a), the blue ellipse indicates a 95% level confidence set for a decision maker in our dataset.

[Figure 3 about here.]

An immediate consequence of Lemma 2.1 is that a direct comparison of the sample estimate $(\hat{\alpha}_H, \hat{\beta}_H)$ with the machine ROC curve is likely to be insufficient. Consider a situation where the true population pair of (α_H, β_H) lies strictly below the machine ROC curve: $\beta_H < g(\alpha_H)$ where $g(\cdot)$ denotes the machine ROC curve. Then with probability converging to 1, $(\hat{\alpha}_H, \hat{\beta}_H)$ lies strictly below the machine ROC. Suppose we replace $(\hat{\alpha}_H, \hat{\beta}_H)$ by $(\hat{\alpha}_H, g(\hat{\alpha}_H))$. By Lemma 2.1, $\mathbb{P}(\hat{\alpha}_H \geq \alpha_H) \rightarrow 0.5$. In other words, the replacement point $(\hat{\alpha}_H, g(\hat{\alpha}_H))$ on the ROC curve does not dominate the true population pair of (α_H, β_H) approximately half of the time. A similar situation arises if we replace $(\hat{\alpha}_H, \hat{\beta}_H)$ by $(g^{-1}(\hat{\beta}_H), \hat{\beta}_H)$. In order to provide a probabilistic statement regarding the property of the replacement procedure, a more formal statistical framework is necessary. We consider both a heuristic frequentist approach and a Bayesian approach.

2.3 A heuristic frequentist approach

We initially experiment with a heuristic procedure based on the frequentist principle, the predominant school of thought in statistical inference which typically begins with confidence set construction. The procedure is described as follows.

- Form a confidence set \hat{S} for θ_H . By Lemma 2.1, $n(\hat{\theta}_H - \theta_H)^T \hat{\Sigma}^{-1}(\hat{\theta}_H - \theta_H)$ converges to a Chi-square distribution with two degrees of freedom, where $\hat{\Sigma}$ is any consistent estimator of Σ . A confidence set on this asymptotic distribution is elliptically shaped.
- For each $s = (\alpha_s, \beta_s) \in \hat{S}$, define A_s as the set of points that *dominate* s :

$$A_s = \{\theta = (\alpha, \beta) : \alpha \leq \alpha_s, \beta \geq \beta_s\}. \quad (3)$$

- Define $A = \bigcap_{s \in \hat{S}} A_s$: A is the set of points that dominate all the points in \hat{S} .
- Next, define $\bar{A} = A \cap \text{ROC}$: \bar{A} is the set of points on the machine ROC curve that simultaneously dominate all the points in \hat{S} .

The convention of choosing a large confidence level suggests that the status quo of human decision making is to be replaced by an algorithm only when there is overwhelming evidence from the data indicating the superiority of the algorithm. In our application, we will only consider the machine algorithm to outperform the human decision when $\bar{A} \neq \emptyset$, i.e., when there exists a point on the machine ROC curve that dominates an entire confidence set of the

human decision maker's θ_H parameter. In essence, we use estimates of the sampling uncertainty of the FPR/TPR pair of $\hat{\theta}_H$ to provide guidance on how far $\hat{\theta}_H$ needs to be below the machine ROC curve in order to justify replacing the human decision maker with the machine algorithm.

In the elliptical confidence set depicted in Figure 3(a), denote by $(\alpha_{\beta_{high}}, \beta_{high})$ the point that achieves the highest TPR on the confidence set, and denote by $(\alpha_{low}, \beta_{\alpha_{low}})$ the point that achieves the smallest FPR on the confidence set. The point P in Figure 3(a) corresponds to $(\alpha_{low}, \beta_{high})$. There are three possibilities for the relation between the position of the confidence set for the human FPR/TPR pair θ_H and the machine ROC curve.

1. Case 1 (Figure 3(a)): The human confidence set and point $P = (\alpha_{low}, \beta_{high})$ are both below the machine ROC curve. We consider the human decision maker to perform “worse” than the algorithm and hence can be replaced by the algorithm. On the machine ROC curve, we can find two points, namely, (α_R, β_{high}) and (α_{low}, β_R) , labeled as points B and A in Figure 3(a), such that any point on the ROC curve between A and B can provide a machine decision rule to replace human decision making.
2. Case 2 (Figure 3(b)): The entire human confidence set is below the ROC curve, but the point $P = (\alpha_{low}, \beta_{high})$ is above the ROC curve. In this case, even though each point in the confidence region of θ_H is dominated by some point on the machine ROC curve, it is not possible to find a nonempty fraction of the machine ROC curve that simultaneously dominates all the points in the human confidence set. The data evidence is not sufficiently convincing to account for the randomness of estimating θ_H by $\hat{\theta}_H$. Consequently, the human decision maker is not replaced by the algorithm.
3. Case 3 (Figure 3(c)): The human confidence set has a certain area above the machine ROC curve. The human decision maker is not replaced by the algorithm either.

In summary, if the point $P = (\alpha_{low}, \beta_{high})$ is below the ROC curve, the human decision maker is replaced; otherwise, they are not. In cases 2 and 3, it is possible that the human decision maker is sufficiently capable compared to the machine algorithm. It is also possible that the human θ_H is not estimated precisely enough, for example, due to a lack of historical data that results in a large confidence set.

In frequentist statistical inference, θ_H is a fixed number. It is either above or below the machine ROC curve. The confidence set itself \hat{S} is a random set, such that $\mathbb{P}(\theta_H \in \hat{S}) \rightarrow 1 - \alpha$. For a conventional size of $\alpha = 0.05$, if the confidence set is to be constructed 100 times from different samples, \hat{S} will contain θ_H approximately 95 times. Consequently, by construction, \bar{A} is a random set such that asymptotically,

$$\mathbb{P}(\theta_H \in \hat{S}) = \mathbb{P}\{\bar{A} = \emptyset \text{ and P dominates } \theta_H\} + \mathbb{P}\{\bar{A} \neq \emptyset \text{ and } \bar{A} \text{ dominates } \theta_H\} \geq 1 - \alpha.$$

Therefore, we have asymptotically

$$\mathbb{P}\{\bar{A} \text{ dominates } \theta_H | \bar{A} \neq \emptyset\} \geq \frac{1 - \alpha - \mathbb{P}\{\bar{A} = \emptyset \text{ and P dominates } \theta_H\}}{\mathbb{P}\{\bar{A} \neq \emptyset\}}.$$

If θ_H lies below the ROC curve, $\mathbb{P}\{\bar{A} = \emptyset\} \rightarrow 0$ as the number of cases for the human decision maker increases to infinity. Furthermore, $\mathbb{P}\{\bar{A} = \emptyset \text{ and P dominates } \theta_H\} < \mathbb{P}\{\bar{A} = \emptyset\} \rightarrow 0$, implying that asymptotically, $\mathbb{P}\{\bar{A} \text{ dominates } \theta_H | \bar{A} \neq \emptyset\} \geq 1 - \alpha$. If θ_H lies above the ROC, we can control $\mathbb{P}\{\bar{A} = \emptyset\} \geq 1 - \alpha$ by reasoning that

$$\mathbb{P}\{\bar{A} = \emptyset\} = \mathbb{P}\{\text{P is above ROC}\} \geq \mathbb{P}\{\text{P dominates } \theta_H\} \geq \mathbb{P}(\theta_H \in \hat{S}) \geq 1 - \alpha.$$

However, the finite sample size of the test can be severely distorted. By insisting on finding a segment of the machine ROC curve that simultaneously dominates the entire confidence region of θ_H , the frequentist procedure is conservative by construction.

While conventional confidence sets are mostly symmetric, it is well known in statistics that by inverting a hypothesis test, alternative confidence sets can be constructed as the collection of parameter values for which the null hypothesis is not rejected. For example, if we let the null hypothesis be $H_0 : \theta_H = \theta_{0H}$ and the alternative hypothesis be $H_1 : \alpha_H > \alpha_{0H}$ or $\beta_H < \beta_{0H}$, a test can be formed to reject the null hypothesis H_0 when either $\hat{\alpha}_H > \alpha_H + c$ or when $\hat{\beta}_H < \beta_H - d$, where c and d are chosen by the size of the test. The confidence set of θ_{0H} where the test does not reject takes the form of $\{\theta_{0H} : \alpha_{0H} \geq \hat{\alpha}_H - c, \text{ and } \beta_{0H} \leq \hat{\beta}_H + d\}$, which is lower rectangular. While forming confidence sets based on inverting inequality tests is theoretically intriguing, it is not often used empirically.

An alternative in Appendix A.3 is to test whether the population value of θ_H is above or below the machine ROC curve. We do not use this test because of its limitation that even if the null hypothesis of the status quo of human decision making is rejected, it does not locate a point of the machine ROC curve to replace human decisions, as discussed in section 2.2.

2.4 A Bayesian approach

In the following we focus on an alternative Bayesian method, which often allows for a more transparent interpretation than frequentist inference. The Bayesian approach combines a prior distribution of the underlying population parameters with the likelihood of the data given the population parameters to produce a posterior distribution of the parameters given the data, which is then used in a decision theoretic framework where a threshold is chosen to minimize the posterior expected loss function. The combination of a multinomial likelihood function with a Dirichlet conjugate prior drastically improves computability. Simulating the posterior distribution of the key FPR/TPR parameters to construct a Bayesian credible set is facilitated by writing them as a vector function of the multinomial parameters whose posterior

distribution is given analytically through the conjugate prior. The empirical results suggest that the Bayesian method is less conservative and suggests replacement of more doctors by the machine algorithm than the frequentist method does.

Computing a Bayesian posterior distribution requires two key inputs: the likelihood of the data given the population value of θ_H , and a prior distribution for the underlying population parameters. Each observation in the dataset consists of both the doctor diagnoses and the ground truth of pregnancy outcomes, and follows a multinomial distribution with four categories: diagnosed as risky and abnormal birth outcome; not diagnosed as risky and abnormal birth outcome; diagnosed as risky and normal birth outcome; not diagnosed as risky and normal birth outcome. The parameters of the multinomial probabilities are:

$$t_1 = \mathbb{E}Y\hat{Y}, \quad t_2 = \mathbb{E}\left[(1 - Y)\hat{Y}\right], \quad t_3 = \mathbb{E}\left[Y(1 - \hat{Y})\right], \quad t_4 = \mathbb{E}\left[(1 - Y)(1 - \hat{Y})\right].$$

Since $t_1 + t_2 + t_3 + t_4 = 1$, we choose the first three as free parameters. The multinomial distribution is a completely specified parametric model and allows for exact likelihood Bayesian posterior distribution computation. The likelihood of the data given the free parameters $t = (t_1, t_2, t_3)$ depends only on a set of sufficient statistics $\hat{t} = (\hat{t}_1, \hat{t}_2, \hat{t}_3)$ where

$$\hat{t}_1 = \frac{1}{n} \sum_{i=1}^n Y_i \hat{Y}_i, \quad \hat{t}_2 = \frac{1}{n} \sum_{i=1}^n [(1 - Y_i) \hat{Y}_i], \quad \hat{t}_3 = \frac{1}{n} \sum_{i=1}^n [Y_i (1 - \hat{Y}_i)]. \quad (4)$$

In particular, we can write the data likelihood as (where \mathbb{D} refers to *Data*):

$$L(\mathbb{D}|t) = \binom{n}{n\hat{t}_1} t_1^{n\hat{t}_1} \binom{n - n\hat{t}_1}{n\hat{t}_2} t_2^{n\hat{t}_2} \binom{n - n\hat{t}_1 - n\hat{t}_2}{n\hat{t}_3} t_3^{n\hat{t}_3} t_4^{n(1 - \hat{t}_1 - \hat{t}_2 - \hat{t}_3)}. \quad (5)$$

Given a prior distribution of t , denoted as $\pi(t)$, the posterior distribution of the parameter t , denoted as $p(t|\mathbb{D})$ can usually be simulated or calculated analytically:

$$p(t|\mathbb{D}) = \frac{\pi(t) L(\mathbb{D}|t)}{\int \pi(t') L(\mathbb{D}|t') dt'}.$$

We are interested in the posterior distribution of $\theta_H = (\alpha_H, \beta_H)$, which can be written as functions of the underlying multinomial parameters: $h(t) = (\alpha_H(t), \beta_H(t))$. If we can simulate from the posterior distribution $p(t|\mathbb{D})$ and denote the simulated draws as $t_r, r = 1, \dots, R$, then the posterior distribution of θ_H , denoted as $p(\theta_H|\mathbb{D})$, can be estimated using the empirical distribution of $h(t_r), r = 1, \dots, R$.

Computing the posterior distribution using a multinomial likelihood is facilitated by the Dirichlet conjugate prior. A Dirichlet prior on the K -dimensional simplex of $t_k, k = 1, \dots, K$, where $\sum_{k=1}^K t_k = 1$, is specified by hyper-parameters $\gamma = (\gamma_k, k = 1, \dots, K)$. Its density is given by $\pi(t|\gamma) = \frac{1}{B(\gamma)} \prod_{k=1}^K t_k^{\gamma_k - 1}$, where $B(\gamma)$ is the multivariate Beta function. See for example

Kotz et al. (2019). The case with $\gamma_k = \gamma, \forall k = 1, \dots, K$ is called a symmetric Dirichlet distribution. In one dimension, where $K = 1$, the Dirichlet distribution specializes to a Beta distribution, which in turn includes the uniform distribution as a special case when $\gamma = 1$.

The posterior distribution is also Dirichlet with parameters $\hat{\gamma} = (\hat{\gamma}_k, k = 1, \dots, K)$, where $\hat{\gamma}_k = \gamma_k + n\hat{t}_k$ for each $k = 1, \dots, K$. Simulating from the posterior distribution of $\theta_H = (\alpha_H, \beta_H)$ can be accomplished by recomputing $\theta_{H,r} = h(t_r)$ after drawing for t_r from the posterior Dirichlet distribution with parameters $\hat{\gamma}$. Specifically, for each $t_r = (t_{r,k})_{k=1}^K$, we calculate

$$\begin{aligned} \theta_{H,r} &= h(t_r) = (\alpha_H(t_r), \beta_H(t_r)), \quad \text{where} \\ \alpha_H(t_r) &= \frac{t_{r,2}}{t_{r,2} + t_{r,4}}, \quad \beta_H(t_r) = \frac{t_{r,1}}{t_{r,1} + t_{r,3}}. \end{aligned} \quad (6)$$

The simulated draws $\theta_{H,r}, r = 1, \dots, R$ can be used to estimate posterior probabilities. For example, the posterior probability that θ_H lies below the ROC curve, denoted as

$$\int_{\theta_H \text{ below ROC}} p(\theta_H | \mathbb{D}) d\theta_H, \quad (7)$$

can be estimated by the fraction of times where $\theta_{H,r}$ lies below the ROC curve:

$$\frac{1}{R} \sum_{r=1}^R \mathbb{1}(\theta_{H,r} \text{ lies below the machine ROC curve}) = \frac{1}{R} \sum_{r=1}^R \mathbb{1}(\beta_H(t_r) \leq g(\alpha_H(t_r))).$$

We are mainly interested in the *maximum* posterior probability of θ_H that are *dominated* simultaneously by a single point on the ROC curve, denoted as

$$q_{max} \equiv \max_{\alpha \in [0,1]} \int_{\alpha_H \geq \alpha, \beta_H \leq g(\alpha)} p(\theta_H | \mathbb{D}) d\theta_H, \quad (8)$$

and the corresponding maximizing point, denoted as $\theta_{max} = (\alpha_{max}, \beta_{max} = g(\alpha_{max}))$, where

$$\alpha_{max} \equiv \arg \max_{\alpha \in [0,1]} \left\{ \int_{\alpha_H \geq \alpha, \beta_H \leq g(\alpha)} p(\theta_H | \mathbb{D}) d\theta_H \right\}. \quad (9)$$

Both (8) and (9) can be estimated by the simulated posterior draws of $\theta_{H,r}, r = 1, \dots, R$, by

$$\begin{aligned} \hat{q}_{max} &= \max_{\alpha \in [0,1]} \frac{1}{R} \sum_{r=1}^R \mathbb{1}(\alpha_H(t_r) \geq \alpha, \beta_H(t_r) \leq g(\alpha)), \\ \hat{\alpha}_{max} &= \arg \max_{\alpha \in [0,1]} \sum_{r=1}^R \mathbb{1}(\alpha_H(t_r) \geq \alpha, \beta_H(t_r) \leq g(\alpha)). \end{aligned} \quad (10)$$

More generally, decision-theoretic Bayesian analysis minimizes posterior expected losses.

Let $\rho(\theta_M, \theta_H)$ denote a loss function that represents the disutility of replacing a human FPR/TPR pair θ_H by a machine FPR/TPR pair θ_M . Consistent with Assumptions 1 and 2, we specify $\rho(\theta_M, \theta_H) = 0$ when $\alpha_M \leq \alpha_H$ and $\beta_M \geq \beta_H$, or when the machine FPR/TPR pair strictly dominates the human FPR/TPR pair. Otherwise, $\rho(\theta_M, \theta_H)$ may be strictly positive. Given the choice of $\rho(\theta_M, \theta_H)$, a point on the ROC curve can be chosen to minimize the posterior expected loss

$$\theta_M^0 = \arg \min_{\theta_M: \beta_M = g(\alpha_M)} \int \rho(\theta_M, \theta_H) p(\theta_H | \mathbb{D}) d\theta_H, \quad (11)$$

which is also estimated using the simulated posterior draws of $\theta_{H,r}$, $r = 1, \dots, R$ as

$$\hat{\theta}_M^0 = \arg \min_{\theta_M: \beta_M = g(\alpha_M)} \frac{1}{R} \sum_{r=1}^R \rho(\theta_M, \theta_{H,r}).$$

In particular, (8) is a special case of (11) when $\rho(\theta_M, \theta_H) = 1 - \mathbf{1}(\alpha_H \geq \alpha_M, \beta_H \leq \beta_M)$. It is also possible to explore more general loss functions. For example, we may weight the loss of replacing θ_H by θ_M by the distance between θ_H and the machine ROC curve:

$$\rho(\theta_M, \theta_H) = 1 - \mathbf{1}(\alpha_H \geq \alpha_M, \beta_H \leq \beta_M) \cdot \inf_{\theta} \{\|\theta_H - \theta\| : \theta \text{ on ROC}\}, \quad (12)$$

where $\|\cdot\|$ is the Euclidean norm. Intuitively, the farther a human FPR/TPR pair θ_H is from the ROC curve, the smaller the loss (or the larger the benefit) of replacing it with a *dominating* point on the machine ROC curve. Alternatively, we can replace the distance from θ_H to the ROC curve by the distance of each θ_M to the complement of the set of FPR/TPR points that dominate θ_H , and use the loss function:

$$\rho(\theta_M, \theta_H) = 1 - \mathbf{1}(\alpha_H \geq \alpha_M, \beta_H \leq \beta_M) \cdot \min(\alpha_H - \alpha_M, \beta_M - \beta_H). \quad (13)$$

The Euclidean distance from the machine ROC curve may also not fully capture the loss of not replacing a human FPR/TPR pair θ_H that lies under the machine ROC curve. For example, a diagonal ROC curve corresponds to completely randomized decision making without using feature information. Similarly, a ROC curve below the diagonal can be generated by a decision rule that awards rather than penalizes mis-classification errors. These considerations suggest that replacing a human FPR/TPR pair θ_H below the diagonal line with a dominating θ_M along the machine ROC curve should not entail losses. We can adopt a convention of normalizing the loss to be 1 when θ_M does not dominate θ_H , i.e., when $\alpha_M \geq \alpha_H$ or $\beta_M \leq \beta_H$.

We then specify the loss $\rho(\theta_M, \theta_H)$ when θ_M dominates θ_H and when θ_H lies between the machine ROC curve and the diagonal line. Each of such θ_H can be reproduced by a convex combination of a point on the machine ROC curve and a point on the diagonal line, using

a decision rule that randomizes between the point on the machine ROC curve and the point on the diagonal. For example, $(\alpha_H, g(\alpha_H))$ is generated by a machine based decision rule $\hat{Y}_i = \mathbb{1}(m(X_i) > c_0)$ for some threshold c_0 , while (α_H, α_H) is generated by a fully randomized decision $\hat{Y}_i = \mathbb{1}(U_i \geq 1 - \alpha_H)$ where U_i is independently uniformly distributed on $(0, 1)$. Then (α_H, β_H) can be generated by a lottery that places weight $(\beta_H - \alpha_H) / (g(\alpha_H) - \alpha_H)$ on $\hat{Y}_i = \mathbb{1}(m(X_i) > c_0)$ and the remaining weight on $\hat{Y}_i = \mathbb{1}(U_i \geq 1 - \alpha_H)$. More precisely, if V_i denotes an independent random variable uniformly distributed on $(0, 1)$, the decision rule

$$\hat{Y}_i = \mathbb{1}\left(V_i \leq \frac{\beta_H - \alpha_H}{g(\alpha_H) - \alpha_H}\right) \mathbb{1}(m(X_i) > c_0) + \mathbb{1}\left(V_i > \frac{\beta_H - \alpha_H}{g(\alpha_H) - \alpha_H}\right) \mathbb{1}(U_i > 1 - \alpha_H)$$

generates the (α_H, β_H) FPR/TPR pair. The larger the weight $\lambda_{\theta_H} \equiv \frac{\beta_H - \alpha_H}{g(\alpha_H) - \alpha_H}$ placed on the machine ROC curve, the smaller the benefit, or the larger the loss, of replacing θ_H with a dominating pair θ_M on the machine ROC curve. The randomization scheme motivates using the weight λ_{θ_H} as a component of the loss function

$$\rho(\theta_M, \theta_H) = 1 - \mathbb{1}(\alpha_H \geq \alpha_M, \beta_H \leq \beta_M) (1 - \max\{\lambda_{\theta_H}, 0\}). \quad (14)$$

Other randomization schemes can also be used. We refer to the above construction as a vertical decomposition. Similarly, a horizontal decomposition replaces the weights by $\lambda_{\theta_H} \equiv \frac{\beta_H - \alpha_H}{\beta_H - g^{-1}(\beta_H)}$. In addition, we experiment with decomposing the distance between $\theta_M = (\alpha_M, \beta_M)$ and the diagonal line into two parts. The first part is the distance from θ_M to the boundary of the set of FPR/TPR points that do not dominate θ_H . The second part is the distance from this boundary to the diagonal line. The corresponding loss function that mirrors is

$$\rho(\theta_M, \theta_H) = 1 - \mathbb{1}(\alpha_H \geq \alpha_M, \beta_H \leq \beta_M) (1 - \max\{\lambda_{\theta_H, \theta_M}, 0\}), \quad (15)$$

where distance can be measured either horizontally, implying that $\lambda_{\theta_H, \theta_M} = \frac{\beta_M - \alpha_H}{\beta_M - \alpha_M}$, or vertically, implying that $\lambda_{\theta_H, \theta_M} = \frac{\beta_H - \alpha_M}{\beta_M - \alpha_M}$.

When $\alpha_M < \alpha_H$ and $\beta_M > \beta_H$, replacing θ_H by θ_M is beneficial. The benefit, $b(\theta_M, \theta_H)$, is likely to be larger when θ_H is farther below the machine ROC curve. When either $\alpha_M > \alpha_H$ or $\beta_M < \beta_H$, we expect a cost $\ell(\theta_M, \theta_H)$. A general loss function consists of both a cost component and a benefit component:

$$\rho(\theta_M, \theta_H) = \mathbb{1}(\alpha_H < \alpha_M \text{ or } \beta_H > \beta_M) \ell(\theta_M, \theta_H) - \mathbb{1}(\alpha_H \geq \alpha_M, \beta_H \leq \beta_M) b(\theta_M, \theta_H). \quad (16)$$

For each loss function, a guardrail threshold is used to account for the status quo of human decision making. A human decision maker is only replaced by the machine algorithm when the posterior expected loss of the replacement is below a given prespecified level, or when the posterior expected benefit exceeds a certain level.

In addition to the deterministic decision rules of relying exclusively on either an individual doctor or the machine algorithm, randomized decision rules can be generated by mixing between a given point on the machine ROC curve and an individual doctor. Let ω denote the randomizing probability of using the machine algorithm, and $1 - \omega$ the corresponding probability of relying on the human decision makers. The minimized expected posterior loss of the randomized decision rule can be written as

$$\min_{\omega \in [0,1], \theta_M: \beta_M = g(\alpha_M)} \int \rho(\omega\theta_M + (1 - \omega)\theta_H, \theta_H) p(\theta_H | \mathbb{D}) d\theta_H. \quad (17)$$

Without expert domain knowledge of medical diagnoses, it is difficult to implement (16) and (17). Investigating expert domain knowledge is beyond the scope of the current paper.

Our decision framework differs conceptually from the minimization of posterior expected loss function in Bayesian point estimation. A Bayesian point estimator of θ_H , denoted as $\hat{\theta}_{H,B}$, is often defined as the minimizer of an expected posterior loss function:

$$\hat{\theta}_{H,B} = \arg \min_{\theta \in [0,1]^2} \int \ell(\theta - \theta_H) p(\theta_H | \mathbb{D}) d\theta_H.$$

The estimation loss function $\ell(\theta - \theta_H)$ typically depends only on $|\theta - \theta_H|$ and is increasing in $|\theta - \theta_H|$, which is different from our decision loss function $\rho(\theta_M, \theta_H)$.

2.5 Discussion: incentives and costs

The visual illusion shown in Figure 1 that hampers the comparison between machine learning algorithms and human decision makers is an immediate artifact of Jensen’s inequality. An optimal ROC generated by a correctly specified propensity score function is necessarily concave, since it is the primal function of a concave program. See for example Feng et al. (2022). For the j th doctor, denote the FPR as $\alpha_j = \mathbb{E}(1 - Y_{ij}) \hat{Y}_{ij} / (1 - p_j)$ and the TPR as $\beta_j = \mathbb{E}Y_{ij} \hat{Y}_{ij} / p_j$, where $p_j = \mathbb{P}(Y_j = 1)$. If all the (α_j, β_j) pairs lie on a strictly concave ROC curve $g(\cdot)$, these variables are related by $\beta_j = g(\alpha_j)$. When the patient cases across doctors are drawn from the same population, $p_j = p$ is a constant. It follows from Jensen’s inequality that

$$\bar{\beta} = \frac{1}{J} \sum_{j=1}^J \beta_j = \frac{1}{J} \sum_{j=1}^J g(\alpha_j) < g\left(\frac{1}{J} \sum_{j=1}^J \alpha_j\right) = g(\bar{\alpha}),$$

when α_j are not all equal. This important observation appears to have gone largely unnoticed by the literature. Similarly, if each patient i is diagnosed using a point on the human ROC

curve $(\alpha_{i,j}, \beta_{i,j})$ and if $\alpha_{i,j}, i = 1, \dots, n_j$, are not all equal, it is also the case that

$$\beta_j = \frac{1}{n_j} \sum_{i=1}^{n_j} \beta_{i,j} = \frac{1}{n_j} \sum_{i=1}^{n_j} g(\alpha_{i,j}) < g\left(\frac{1}{n_j} \sum_{i=1}^{n_j} \alpha_{i,j}\right) = g(\alpha_j).$$

Lemma A.2 in the supplementary appendix provides a set of primitive conditions under which the aggregate human decision maker FPR/TPR lies strictly below the machine ROC curve.

In general, without the restrictions in Assumptions 1 and 2, the decision maker j may use a model $\hat{y} = \mathbb{1}(q_j(x, u) > c_j(x, u))$. For decision maker j minimizing expected loss of misclassification conditional on the feature x and u , consider the following loss matrix:

Loss matrix	$\hat{y} = 0$	$\hat{y} = 1$
$y = 0$	0	$c_{01}(x, u)$
$y = 1$	$c_{10}(x, u)$	0

where the misclassification losses c_{01} and c_{10} are now dependent on x and u . Equivalently, decision maker j also minimizes the ex ante expected loss:

$$\mathbb{E} \left[c_{10}(X, U) q_j(X, U) (1 - \hat{Y}) + c_{01}(X, U) (1 - q_j(X, U)) \hat{Y} \right].$$

The optimal decision rule is $\mathbb{1}\left(q_j(x, u) > \frac{c_{01}(x, u)}{c_{10}(x, u) + c_{01}(x, u)} =: c_j(x, u)\right)$. Consequently, for $(x_1, u_1), (x_2, u_2)$ sharing the same propensity score $q_j(x_1, u_1) = q_j(x_2, u_2)$, the choice of the decision maker can be different due to cost differences: $c_j(x_1, u_1) \neq c_j(x_2, u_2)$. Such a decision rule is considered in Elliott and Lieli (2013). Even if all doctors have full information processing capacity, so that $q_j(x, u) = p(x, u)$ for a correctly specified propensity function $p(x, u)$, an arbitrary FPR/TPR pair below the machine ROC curve can still be rationalized by some decision rule $\hat{y} = \mathbb{1}(p(x, u) > c_j(x, u))$ corresponding to a reverse-engineered cost function $c_j(x, u)$.

To illustrate using a synthetic example without u , let x be uniformly distributed on $(0, 1)$ and $p(x) = x$. Let the cutoff threshold function be

$$c(x) = \begin{cases} 0, & x < 1/4; \\ 2(x - 1/4), & 1/4 < x < 3/4; \\ 1, & x > 3/4. \end{cases}$$

Then $\hat{y} = \mathbb{1}(x < \frac{1}{2})$ and $(\text{TPR}, \text{FPR}) = (1/8, 3/8)$, which lies strictly below the diagonal line. An example when the feature may enter into the cutoff threshold is bank lending, where $y \in \{0, 1\}$ denotes whether a loan is paid back, and $\hat{y} \in \{0, 1\}$ denotes whether a loan application is approved. The amount of principal and interests are features x that are likely to affect the probability $p(x)$ of defaulting by the borrower, but that are also likely to affect the cost perception $c(x)$ by the lender. Assumption 1 essentially excludes such difficulty of interpreting

a FPR/TPR pair arising from incentive heterogeneity.

To understand whether the cost perception of doctors might vary systematically with the risk level of their patients, we use the FPR rank for each doctor to measure the conservativeness of their diagnoses. Doctors may be more willing to tolerate a higher FPR for higher risk patients when they perceive riskier patients as less healthy and more likely to incur a higher cost of underdiagnosis. We then estimate the correlation between the FPR ranks and a pregnancy risk level indicator. In particular, we regress $q_{i,j}$, the predicted abnormal birth rate for patients diagnosed by doctor j from a random forest algorithm described in section 3, against r_j , the doctor’s FPR rank:

$$q_{i,j} = \beta_0 + \beta_1 r_j + \epsilon_{i,j}.$$

The doctors’ FPR rank are normalized to $[0, 1]$. If the FPR of doctor j is higher than 80% of the doctors, then $r_j = 0.8$. The regression results for doctors with no less than 300 diagnoses and for doctors with no less than 500 diagnoses are summarized in Table 1. The regression results suggest that there is no strong evidence that the FPR rank of doctors is associated with the risk level of their patients.

[Table 1 about here.]

The use of statistical significance as a benchmark for comparing doctors with the machine algorithm is motivated by the difficulty of fixating a social cost function, even if we assume that informed human decision makers are fully rational and impose strong functional form assumptions. Designing a social loss function empirically relies on the domain knowledge of the specific decision maker. Our replacement algorithm allows for the choice of the cutoff threshold to be specific to each individual doctor, and does not require a homogeneous preference function to be applied to all doctors. The baseline comparison between true positive rates and false positive rates can also potentially mask the severity of individual cases, the identification of which requires a richer dataset with more precise measurements on the outcome variable. While these information are not available in our dataset, exploring richer data information can be a fruitful future direction of research.

A responsible phase-in protocol based on multiple years of data on performance observations can incorporate long term health and wellbeing outcomes into the definition of performance and quality for decision making. Our data is cross-sectional and does not follow doctors or patients over time. When a panel data becomes available in which doctors and patients can be observed over multiple time periods, future work can potentially generalize the current approach to allow for sequential testing and decision making. The challenge of accounting for longer term health outcomes is partially reflected by the current strategy that replaces a doctor’s diagnosis by the machine algorithm only when there is overwhelming statistical evidence suggesting the superiority of the machine decision.

3 Data and Algorithm Description

Our data came from the National Free Prepregnancy Checkups (NFPC) project. Starting from 2010, NFPC offers free health checkup for couples planning to conceive and is conducted across 31 provinces in China. The dataset contains more than 300 features for each observation, including age, demographic characteristics, results from medical examinations and clinical tests, disease and medication history, pregnancy history, lifestyle and environmental information of both wives and husbands. The data also include the birth outcome, which is denoted as normal ($y = 0$) or abnormal ($y = 1$). In addition, the dataset records doctors' IDs and diagnoses of pregnancy risk. The doctors' diagnoses are graded according to 4 levels: 0 for normal, 1 for high-risk wife, 2 for high-risk husband, and 3 for high-risk wife and husband. In this paper, we group the doctor's diagnoses into 2 categories, where a grade of 0 corresponds to normal pregnancy and any higher grade corresponds to a diagnosis of risky pregnancy.

Our original dataset includes 3,330,304 couples that have pregnancy outcomes between January 1, 2014, and December 31, 2015. We exclude duplicate features and samples for which either doctors' diagnoses or more than 50% of feature values are missing. We were left with 168 features of 1,137,010 couples who were diagnosed by 28,716 doctors. Of these observations, 61,184 couples (5.38%) had abnormal birth outcomes.

A basic measurement of the prediction quality of a binary classifier is accuracy, which is the proportion of correct predictions. However, accuracy itself is inadequate in many applications. As the adverse birth rate is about 5%, a naive classifier that categorizes all cases as low risk would achieve an accuracy of nearly 95%. This is clearly controversial. The doctors' overall accuracy is 73.63%, and 24.04% of pregnancies are diagnosed as high-risk. Doctors' aggregate false positive rate and true positive rate are 0.2379 and 0.2843. In contrast, the FPR and TPR of the naive predictor are both zero. In other words, doctors are willing to tolerate a higher FPR in order to achieve a higher TPR.

We focus on doctors who diagnosed more than 300 patients. There are 584 such doctors corresponding to 584,181 patient cases. Using a ratio of 7:3 and stratification methods, we randomly split our sample into a classification set and a performance set. We use the classification set to train a machine learning algorithm, and then we categorize a doctor as "replaced" or "retained" according to our statistical procedure. The performance set is used to compute the FPR/TPR of the combined diagnoses. The data cases are stratified into the four classes based on the actual birth outcomes and the doctors' diagnoses: true positive cases, true negative cases, false negative cases and false positive cases. The random splitting process is performed through each class of data with the same ratio of 7:3. Subsequently, the data in each class are merged to form the classification and performance sets. In total, there are 408,661 cases in the classification set and 175,520 cases in the performance set.

We further split the classification set into two subsets. The first subset is the training set

used to estimate the parameters in a machine learning algorithm. The second subset is the validation set used to evaluate the performance of the algorithm and obtain the machine ROC curve. Splitting of the classification set into the training and validation subsets is done using a ratio of 4:3 and the same stratification method described above. There are 233,435 cases in the training set and 175,226 cases in the validation set.

We experimented with several algorithms. We begin with decision trees, which are widely used in many machine learning applications. However, a single tree method usually has high variance despite its low bias, and tends to overfit by generating results with substantial variation even when a small amount of noise is present in the data. In contrast, random forest (RF) is a commonly used ensemble learning algorithm proposed by [Breiman \(2001\)](#), and overcomes these problems by constructing a collection of decision trees that are trained using different feature subspaces and bootstrapped samples. The predictions of each tree are aggregated to make predictions. [Appendix A.2](#) provides more details about the random forest algorithm.³

Remark 1. The classification of doctors’ diagnoses by both husband and wife raises a question regarding the validity of [Assumption 1](#) that rules out intra-individual incentive heterogeneity, if the relative costs of false positives to false negatives differ between when a single person is deemed risky and when both are deemed risky. A multiclass classification model with four outcome labels differentiating abnormal pregnancy outcomes due to high risks in wife, husband and both spouses can allow for heterogeneous relative costs of false positives to false negatives across these cases. However, in our dataset, the outcome label is only binary indicating whether the birth is classified as normal or abnormal. The lack of the corresponding four-way outcome label makes it difficult to compute an accurate TPR and FPR for each of the diagnosis class.

As an illustration, we empirically calculate the FPR/TPR using the binary outcome label for each of the four diagnosis cases, and report the aggregate summary in the following table:

[Table 2 about here.]

On the one hand, in Panels A and B of [Table 2](#), there are some differences between the TPRs and FPRs among the three diagnosing classes of high risk wife, husband and both spouses. However, without the corresponding outcome level it is difficult to interpret these ratios since the total number of abnormal births used in calculating the denominators aggregates the three unobserved latent outcome labels corresponding to high risk wife, husband and both spouses.

On the other hand, Panel C of [Table 2](#) reports the precision for each of the three diagnosis classes (high risk wife, husband and couple). Precision is defined as the fraction of abnormal birth for each of the diagnosis classes. For example, wife (husband) precision represents the fraction of couples with a high risk wife (husband) diagnosis who have an abnormal birth

³We choose the following parameter settings. The number of estimators N is 100. The number of max features per node M is 50. The minimum number of samples required to split is 50.

outcome. Couple precision is similarly defined. In Panel C of Table 2, the precision parameters for different diagnosis classes are close to each other. The precision parameters, despite being an imperfect measurement, provide a more accurate indication suggesting that the relative costs of false positives to false negatives are not different between cases when a single person is deemed risky and when both are.

4 Empirical Results for AI and doctor decision making

This section presents the empirical results from the heuristic frequentist approach described in section 2.3 and the Bayesian approach described in section 2.4. Doctors who are not replaced by the machine algorithm are called retained doctors hereafter.

4.1 Results of the heuristic frequentist approach

The frequentist approach identifies a dominating segment of the machine ROC for machine algorithm classification. The quality of machine algorithm classification is evaluated by averaging over a uniform grid of points on this dominating segment. For each doctor, we obtain the 95% elliptical confidence area of θ_H centered around the sample estimates using an estimate of the asymptotic covariance matrix based on 100 bootstrap samples. We find the largest TPR point $(\alpha_{\beta_{high}}, \beta_{high})$ and the smallest FPR point $(\alpha_{low}, \beta_{low})$ of the confidence set. The reference point of the doctor is then given by $P = (\alpha_{low}, \beta_{high})$, as shown in Figure 3(a), which is used to classify doctors into two groups. When a doctor’s reference point P is below the machine ROC curve, corresponding to case 1 in section 2.3, the doctor is replaced by the algorithm. When a doctor’s reference point P is above the machine ROC curve, corresponding to cases 2 or 3 in section 2.3, either because this doctor is more capable than the algorithm or this doctor’s capability cannot be precisely measured due to fewer patient observations and a larger confidence set, the doctor is retained in decision making.

Among the 584 doctors, 175 doctors are classified by the frequentist approach as replaced by the algorithm. Consequently, patient cases in the performance set are diagnosed by 175 machine doctors (30.0%) and 409 (70.0%) human doctors. For each of the replaced doctors, $N = 100$ points on the dominating segment of the machine ROC curve are chosen corresponding to a uniform grid of the threshold value c for the algorithm to make classification decisions, as summarized in Appendix A.3. Figure 4 shows the results of this experiment. The aggregate FPR/TPR pair of all doctors on the performance set, represented by the blue point, is 0.2065 for FPR and 0.2264 for TPR. The ROC curve of the random forest model on the performance set is the green curve. The area under the curve (AUC) is 0.6851.

The yellow point uses a decision threshold c corresponding to the upper endpoint of the dominating segment of the machine ROC curve associated with a highest FPR/TPR pair of 0.2017 and 0.3326. Compared to the raw data where all diagnoses are performed by doctors,

the yellow point increases the TPR by 46.9% and reduces the FPR by 2.3%. The green point corresponds to the lower endpoint of the dominating segment of the machine ROC curve and is associated with a lowest FPR/TPR pair of 0.1836 and 0.2974. Compared to the aggregate doctor diagnoses, the green point increases the TPR by 31.4% and reduces the FPR by 11.1%.

[Figure 4 about here.]

The cyan interval in Figure 4 reflects a trade-off between improving the TPR and reducing the FPR. Any point along the interval represents an enhancement over the aggregated doctors' FPR/TPR pair. Furthermore, the red point achieves the maximum F1 score⁴ of 0.1309 along the dominating segment of the machine ROC curve. Figure 5 is a scatter plot of the FPR/TPR pairs of both replaced and retained doctors against the ROC curve in the performance dataset. We see that two adjacent points can be of different replacement status. This can be due to different numbers of patients treated or the use of the test set for calculating the FPR/TPR pairs. An important caveat is that our test depends crucially on the sample size of the number of patients treated by each doctor, which introduces an implicit bias that favors experimenting with junior doctors until the null hypothesis that a doctor is not to be replaced is rejected with sufficient evidence from seeing a large number of patient cases.

[Figure 5 about here.]

When the quality of the stock of decision makers may evolve over time, allowing the juniors to learn from making potentially suboptimal decisions for their patients has the potential of increasing the future pool of high quality seniors. This is likely to be a very delicate issue involving complex welfare tradeoff between current and future generations of patients.

4.2 Results of the Bayesian approach

The prior distribution $\pi(t)$ is chosen to be a symmetry Dirichlet distribution with the parameters $(\gamma_1, \gamma_2, \gamma_3, \gamma_4)$ all set to $\gamma = 0.01$. For doctor j 's i th patient case, \hat{Y}_{ij} is the doctor's diagnosis and Y_{ij} is the ground-truth label of pregnancy outcome. The likelihood for data is given in (5) where \hat{Y}_i , Y_i and n in (4) are replaced by \hat{Y}_{ij} , Y_{ij} and n_j . The posterior distribution is also a Dirichlet distribution with parameters $(\hat{\gamma}_1, \hat{\gamma}_2, \hat{\gamma}_3, \hat{\gamma}_4)$ where $\hat{\gamma}_k = \gamma + n\hat{t}_k$ for $k = 1, 2, 3, 4$. The posterior distribution of $\theta_H = (\alpha_H, \beta_H)$ can be simulated in a two step procedure. In the first step, R samples of $\{t_r = (t_{1r}, t_{2r}, t_{3r}, t_{4r})\}_{r=1}^R$ are drawn from the posterior Dirichlet distribution with parameters $(\hat{\gamma}_1, \hat{\gamma}_2, \hat{\gamma}_3, \hat{\gamma}_4)$. In the second step, we compute $\{\theta_{H,r} = (\alpha_H(t_r), \beta_H(t_r))\}_{r=1}^R$ with the simulated R samples of $t_r, r = 1, \dots, R$, using (6).

⁴The F1 score is the harmonic average of precision and recall, and is often used as a single measurement that conveys the balance between precision and recall. It is widely used in evaluating the performance of algorithms (see for example [Baeza-Yates et al. \(1999\)](#)).

The simulated draws $\theta_{H,r}, r = 1, \dots, R$ are used to calculate (10). If $\hat{q}_{max} \geq 0.95$, we mark the doctor as replaced. The threshold c that corresponds to the point $(\hat{\alpha}_{max}, g(\hat{\alpha}_{max}))$ given by (10) is used as the decision threshold for the algorithm. In Figure 6(a), the maximum coverage rate $\hat{q}_{max} = 0.9657$ at the black point on the machine ROC curve. The doctor is replaced by the algorithm. In Figure 6(b), the maximum coverage rate $\hat{q}_{max} = 0.3179$. There is not sufficient evidence to replace the doctor’s decisions with the algorithm’s.

[Figure 6 about here.]

Figure 7(a) shows the experiment results for doctors who had diagnosed more than 300 cases. A total of 269 (46.1%) out of 584 doctors are classified as replaced. The remaining 315 (53.9%) are retained human doctors. The combined decisions by the retained human doctors and the algorithm’s decisions indicated in the figure by the yellow point, result in an FPR of 0.1856 and a TPR of 0.3319, corresponding to an increase of 46.6% in the TPR and a reduction of 10.1% in the FPR. Similar to Figure 5, Figure 7(b) is a scatter plot of the FPR/TPR pairs of both replaced and retained doctors against the ROC curve in the performance dataset.

[Figure 7 about here.]

We experiment with several alternative definitions described in equations (12) to (15) for the Bayesian posterior expected loss functions in (11). These results are shown in Figure 8, where panel (b) magnifies a portion of panel (a) containing the replacement paths. Ranking the doctors by their expected posterior losses allows us to replace only the doctors whose expected loss of being substituted by the machine algorithm is relatively low. Figure 8 traces the dynamics of the aggregate FPR/TPR pairs of combining the doctor with the machine decisions, when the ratio of replaced doctors increases from 0% to 100%.

[Figure 8 about here.]

In Figure 8(a) legends, *Bayesian Test* refers to the baseline construction in (8); *Euclidean Distance to the ROC curve* refers to the loss function in (12); *Complementary Set Boundary Euclidean Distance* refers to the loss function in (13); *Diagonal Line Horizontal and Vertical Decompositions* refer to the loss function in (14); *Complement Set Boundary Vertical and Horizontal Decompositions* refer to the loss function in (15). No individual loss function demonstrates saliently stronger discriminatory power over the entire replacement path. Furthermore, the incremental benefit going beyond a 50% replacement rate is a small marginal reduction of FPR. In addition, the baseline 95% credible level Bayesian test implemented using (8) is not dominated by any of the competing methods in the FPR/TPR comparison.

The null hypothesis of both the Bayesian analysis and the frequentist analysis is the status quo of human decision making. A human decision maker is replaced by the machine algorithm

only when there is strong evidence from the data favoring the machine algorithm. An alternative conceptual paradigm is to treat the machine algorithm as the status quo null hypothesis, where the human decision makers are by default replaced by the machine algorithm unless there is strong data evidence validating the superiority of human decision making.

However, when we experiment with the alternative specification of the status quo, all except a few doctors are determined to be replaced by the machine algorithm. In the cross-point labeled as the “dominate method” in Figure 9, a doctor is retained if there exists a point on the machine ROC curve that is dominated by at least 95% of the posterior distribution of $p(\theta_H|\mathbb{D})$. A mere 6 doctors are retained in this method. In the cross-point labeled as the “above method” in Figure 9, a doctor is retained if the posterior probability of $p(\theta_H|\mathbb{D})$ above the machine ROC curve is more than 95%. Only 7 doctors are retained using this method. For doctors who are replaced by the machine algorithm, the replacement point on the ROC curve is determined by the baseline Bayesian tests in (10).

[Figure 9 about here.]

At high replacement ratios, the FPR and TPR levels decrease simultaneously across all loss functions. Even when all the doctors are substituted by the machine algorithm, the resulting FPR/TPR pair still lies below the machine ROC curve. This is because different threshold cutoff values on the machine ROC curve are employed to replace different doctors and because of the concavity arguments formalized in Lemma A.2.

On the one hand, in the current empirical dataset, only a small fraction of doctors have FPR/TPR pairs above the machine ROC curve. We have not been able to combine doctors with the machine algorithm to generate a FPR/TPR pair above the machine ROC curve. On the other hand, using a data generating process that allows for a substantial portion of doctors with FPR/TPR pairs to be above machine ROC curve, reported in the synthetic data analysis section 5, we are able to combine the doctors and the machine algorithm to generate a FPR/TPR pair that outperforms even the machine ROC curve.

Instead of deterministically replacing some doctors by the machine algorithm, Appendix A.5 reports the results of a randomized replacement experiment where each replaced doctor accepts the machine decision probabilistically according to a pre-specified acceptance rate $\lambda \in [0, 1]$. As expected, the overall FPR/TPR pairs vary incrementally from when $\lambda = 0$, corresponding to human decision making, to when $\lambda = 1$, corresponding to deterministic replacement of doctors by the machine algorithm.

Appendix A.6 considers a more general form of substitution to replace a subset of patient cases for each doctor. We use patient case covariates to predict the likelihood that the doctor’s diagnoses differ from the ground-truth outcome, and replace only those patient cases where the doctor is prone to make mistakes. While the resulting pattern of the replacement paths is

quite different, the patient-case specific substitution approach does not show saliently stronger discriminatory power compared to the baseline Bayesian approach.

4.3 Characteristics of replaced doctors

Our paper identifies a subset of the doctors to be replaced by the machine algorithms according to FPR/TPR indicators. We create a dummy variable “replaced” that is set to 1 when a doctor is replaced by the algorithm and is set to 0 otherwise, and examine the partial correlation coefficient between the “replaced” dummy variable with several confounding factors including whether they practice in a clinic or hospital.

We regress the “replaced” indicator on three confounding factors. The first factor is county-level per capita GDP (in ten thousand Chinese yuans) collected manually from the statistical yearbooks of 2014 across cities and provinces, which is the starting year of our data⁵. The second factor is the logarithm of the total number of patient cases diagnosed by each doctor. The third factor is represented by two dummy variables related to the practice history of each doctor. A doctor in our dataset may practice in more than one type of facility. The practice facility can be either a county hospital or a township clinic. Medical facilities in China are typically classified by the administrative level that they belong to. On the one hand, urban residents usually go to a county level hospital. On the other hand, rural residents often times go to a township level clinic, which is generally considered to be of lower quality than a county level hospital. The doctors in our data fall into three categories. Doctors who have practiced in both types of facilities are used as the reference level. The first dummy variable representing the third factor is set to 1 for doctors who have practiced only in a county hospital. The second dummy variable representing the third factor is set to 1 for doctors who have practiced only in a township clinic. There are additional variables in the dataset that are only available at a more aggregated the city or province level, such as birth rate and the average number of medical staff. We do not use these variables because, given how administrative units are divided in China, a municipal unit can include many county level units with heterogeneous economic conditions.

The data summary statistics are reported in Panel A of Table 3. As shown in Panel A of Table 3, doctors who have practiced at both a county hospital and a township clinic have seen the largest number of patient cases and have a high replacement ratio. Doctors who have practiced only at a township clinic have seen a smaller number of patient cases compared to doctors who have practiced only at a county hospital, but doctors who have practiced only at a township clinic have a higher replacement ratio than doctors who have practiced only at a county hospital have.

[Table 3 about here.]

⁵The statistical yearbook of year A records the latest available data before year A .

Panel B in Table 3 reports a logistic regression of the replacement indicator on county level per capita GDP and the logarithm of the number of patients seen by the doctor. Column (2) adds an indicator of whether the doctor practices only in a township clinic, and an indicator of whether the doctor practices only in a county hospital. The reference level where both indicators are zero corresponds to doctors who have practiced in both a township clinic and a county hospital. Province fixed effects are included in the logistic regression. We use cluster robust standard errors in order to correct for spatial autocorrelation.

The logistic coefficient estimates do not contradict our a priori reasoning. While higher per capita GDP is associated with a lower likelihood of replacement, the corresponding coefficients are small and lack statistical significance. The coefficients of the log number of patients are positive and statistically significant, indicating the higher distinguishing power of the Bayesian test when a doctor sees more patients. The FPR/TPR pairs of doctors with more patient cases can be estimated more precisely. Consequently, it is more likely for these doctors whose FPR/TPR pairs are below the machine ROC curve to be identified as replaced by our statistical procedure. This finding is consistent with the lack of evidence contradicting Assumption 2 that doctors accumulate experience from additional patient cases.

Doctors practicing only at township clinics have higher replacement probability than reference level doctors practicing at both township clinics and county hospitals, who in turn have higher replacement probability than doctors practicing only at county hospitals. Anecdotal evidence in China suggests that doctors with better medical school records are more likely to be assigned directly to county level hospitals than to have to work their ways up from township clinics into county hospitals.

To distinguish an analysis of the predictors of performance of doctors from the predictors of tests concluding whether they are to be replaced by the machine algorithm, we implement a kernel regression of TPR on FPR and a number of confounding features including county level per capita GDP, the logarithm of the number of patients seen by the doctor, an indicator of whether the doctor practices only in a township clinic, and an indicator of whether the doctor practices only in a county hospital.⁶ Among doctors achieving the same FPR, those achieving a higher TPR can be considered to perform better. A confounding variable with a positive coefficient enhances the TPR after controlling for FPR, and is interpreted as a variable that positively predicts performance.

Panel C in Table 3 reports the results from this regression. The regression coefficients have signs that are consistent with a priori reasoning, but they are also mostly insignificant except for the coefficients on the indicator of whether the doctor practices only in a county hospital. For a given FPR, a higher TPR is positively associated with higher county level per capita GDP, a larger number of patients seen by the doctor and the indicator that the doctor practices only

⁶We thank the associate editor and the review team for suggesting a direct analysis of the performance of doctors.

in a county hospital, but is negatively associated with the indicator that the doctor practices only in a township clinic. The statistical insignificance of the coefficients on the logarithm of the number of treated patients in Panel C of Table 3 and their significance in Panel B of Table 3 provide further evidence that the replacement indicator is largely driven by the difference in the sample size. A larger sample size makes it easier to reject the null hypothesis that the machine algorithm does not outperform the doctor.

5 Synthetic Data Analysis

5.1 An example of human-algorithm complementarity

In our empirical dataset, only a small fraction of doctors lie above the machine ROC curve. Combining the machine algorithm and the doctor decisions results in aggregate FPR/TPR pairs that are still below the machine ROC curve. In addition, Jensen’s inequality (elaborated in section 2.5) likely contributes to the combined aggregate FPR/TPR pair lying below the machine ROC curve. Even if we replace every doctor by the machine algorithm, unless the same point on the machine ROC curve is used to replace all doctors, the combined aggregate FPR/TPR pair is necessarily below the machine ROC curve. The end points of the replacement paths in Figure 8 correspond to replacing all doctors by the machine algorithm. The algorithms that we implemented use different points on the machine ROC curve to replace doctors. These points also differ across different doctors. In order for the combined aggregate FPR/TPR pair to be above the machine ROC curve, it is necessary that a sizable portion of the original doctor diagnoses lie above the machine ROC curve.

While not the case in the NFPC dataset, other datasets might exist where a significant portion of human decision makers correctly use private information not available to the machine algorithm. Figure 10 reports the results from a synthetic data analysis where the combined aggregate FPR/TPR pair between doctors and the machine algorithm lies above the machine ROC curve.

[Figure 10 about here.]

The data generating process of the simulation in Figure 10 is as follows. The input features are three dimensional: $x_{i,j,1}$, $x_{i,j,2}$ and $u_{i,j}$. On the one hand, the first two features, denoted $x_{i,j,1}$ and $x_{i,j,2}$, are assumed to be observable both by the doctors and the machine algorithm. On the other hand, the last feature, denoted $u_{i,j}$, is only observable to the doctors and is not used by the machine algorithm. The three features are generated from independent normal distributions with pre-specified means and variances: $X_{i,j,1} \sim N(0, 1.95)$, $X_{i,j,2} \sim N(0, 0.25)$

and $U_{i,j} \sim N(0, 2)$. The ground truth variable $Y_{i,j} \in \{0, 1\}$ is generated by

$$Y_{i,j} = \mathbb{1}(p(X_{i,j,1}, X_{i,j,2}, U_{i,j}) > \delta_{i,j}) \quad \text{where} \quad p(X_{i,j,1}, X_{i,j,2}, U_{i,j}) = \frac{e^{X_{i,j,1} + X_{i,j,2} + U_{i,j}}}{1 + e^{X_{i,j,1} + X_{i,j,2} + U_{i,j}}}$$

and where $\delta_{i,j}$ is uniformly distributed between 0 and 1. Using this specification of the data generating process, we simulated 600,000 patient cases and allocate them evenly to 2000 doctors. Each doctor is assigned 300 simulated patient cases.

Doctors are partitioned into two groups according to their information processing capacities. The first group, consisting of 750 *more capable* doctors, use the correct full information propensity score $p(x_{i,j,1}, x_{i,j,2}, u_{i,j})$ with different incentives to diagnose patient cases. Their decision rule is given by, using C_j that is uniformly distributed between 0.4 and 1 across doctors,

$$\hat{Y}_{i,j} = \mathbb{1}(p(X_{i,j,1}, X_{i,j,2}, U_{i,j}) > C_j).$$

The second group of doctors, consisting of 1250 *less capable* doctors, use a misspecified propensity score to diagnose patients. Their decision rule is

$$\hat{Y}_{i,j} = \mathbb{1}(q(X_{i,j,1}, X_{i,j,2}, U_{i,j}) > C_j) \quad \text{where} \quad q(X_{i,j,1}, X_{i,j,2}, U_{i,j}) = \frac{e^{-X_{i,j,1} + X_{i,j,2} + U_{i,j}}}{1 + e^{-X_{i,j,1} + X_{i,j,2} + U_{i,j}}}$$

is a misspecified propensity score function.

We divide the 600,000 simulated observations into a training subset consisting of 240,000 observations, a validation subset consisting of 180,000 observations and a test subset consisting of the remaining 180,000 observations. We estimate a random forest model using only the training subset and the first two features $x_{i,j,1}$ and $x_{i,j,2}$, and use the baseline Bayesian test in equation (10) to combine doctors with the machine algorithm. The red point in Figure 10 represents the combination of doctors and the machine algorithm. It lies above the ROC curve of the random forest model, and also strictly dominates the blue point of the aggregate FPR/TPR pair of all doctors. In summary, the synthetic data analysis represented by Figure 10 illustrates the scientific principle of complementarity in human algorithm collaborations. See for example Bansal et al. (2021).⁷

5.2 Aggregating information by predicted doctor models

Our dataset contains doctor diagnoses information in addition to the eventual pregnancy outcomes. In this section we discuss whether estimating a model that predicts the label of doctors' diagnoses can assist in improving the FPR/TPR tradeoff of medical decisions. A model of predicted doctors can be intuitively interpreted as doctors' collective wisdom. The experience

⁷We are grateful to an anonymous referee for pointing us to the science literature on human-algorithm collaboration complementary.

of senior doctors can provide guidance to junior doctors with limited clinical exposures.

In the NFPC dataset, a model of predicted doctors does not appear to improve on the aggregate FPR/TPR pair. However, in several of the following synthetic data examples, a predicted doctor model improves upon the diagnoses of individual doctors. Each doctors' diagnosis may encode information heterogeneity, or incentive heterogeneity, or both. Consider a model of incentive heterogeneity, where doctors' decision rules are given by $\hat{y}_i = \mathbb{1}(p(x_i) > u_i)$ such that $p(x_i)$ is the correctly specified propensity score, and u_i is independently distribution with a strictly monotonic CDF $G(\cdot)$. On the one hand, the aggregate doctor FPR/TPR lies below the optimal ROC curve. On the other hand, the predicted doctor model, given by $\mathbb{E}[\mathbb{1}(p(X_i) > U_i) | X_i] = \mathbb{P}(U_i \leq p(X_i)) = G(p(X_i))$, is a monotonic transformation of the true propensity score function and recovers the optimal ROC curve.

We next focus on several information model without incentive heterogeneity. Consider a baseline example where doctors have access to private information u_i in addition to the publicly observed features x_i and are aware of the correct full information propensity score model $p(x_i, u_i)$. If we could directly observe doctors' probabilistic assessment $p(x_i, u_i)$ and use it as the label to train a machine learning model, then the resulting model will necessarily coincide with the ground-truth machine learned propensity score model:

$$\mathbb{E}[p(X_i, U_i) | X_i] = \mathbb{E}[\mathbb{E}[Y_i | X_i, U_i] | X_i] = \mathbb{E}[Y_i | X_i] = p(X_i).$$

However, in reality we rarely solicit doctors' probabilistic assessment of the likelihood of an illness. Instead, we only observe the binary diagnosis by the doctors, which corresponds to observing $\hat{y}_i = \mathbb{1}(p(x_i, u_i) > c_0)$ for some threshold value c_0 . When we use \hat{y}_i as the label to train a machine learning model, the propensity score of the resulting predicted doctor model is

$$q(X_i) = \mathbb{E}[\mathbb{1}(p(X_i, U_i) > c_0) | X_i].$$

In general, $q(X_i)$ is different from $p(X_i)$. The ROC curve implied by $q(X_i)$ coincides with $p(X_i)$ only when $q(X_i)$ is an increasing transformation of $p(X_i)$: $q(X_i) = \Lambda(p(X_i))$, where $\Lambda(\cdot)$ is a strictly increasing function. There is no guarantee that this is necessarily the case.

Consider now three scenarios in which doctors employ misspecified models to process private information. In the first scenario, doctors process the full information (X_i, U_i) using an incorrect propensity score model $q(X_i, U_i)$, but the ROC curve implied by the predicted doctor model $q(X_i)$ still coincides with the ground-truth machine ROC curve. Figure 11(a) illustrates this scenario using the following data generating process. The ground-truth propensity score model is $p(X_i) = \exp(X_i) / (1 + \exp(X_i))$. The doctors use a misspecified propensity model of $q(X_i, U_i) = \exp(X_i + U_i) / (1 + \exp(X_i + U_i))$. Both X_i and U_i are uniformly and independently distributed: $X_i \sim U(-1, 1)$ and $U_i \sim U(-2, 2)$. The “ X_i only” ROC curve is generated by $p(X_i)$; the “ X_i and U_i ” ROC curve is generated by $q(X_i, U_i)$. The “Predicted Doctors on

X ” ROC curve is generated by $q(X_i) \equiv \mathbb{E}[\mathbf{1}(q(X_i, U_i) > c_0) | X_i]$.

[Figure 11 about here.]

For any given cutoff threshold c_0 , the predicted doctor model $q(X_i)$ is an increasing function of X_i , as is $p(X_i)$. In this particular case, both $p(X_i)$ and $q(X_i)$ correspond to the same ROC curve. This curve lies above the ROC curve generated by $q(X_i, U_i)$ and the aggregate doctor FPR/TPR pair ($c_0 = 0.7$). Collective wisdom improves upon the misspecified model employed by individual doctors and results in higher diagnosing quality as represented by the ROC curves.

The second scenario, pictured in Figure 11(b), is generated by a two dimensional observable feature model. The ground-truth propensity score model is

$$p(X_{i1}, X_{i2}) = \exp(X_{i1} + X_{i2}) / (1 + \exp(X_{i1} + X_{i2})).$$

The doctors’ (misspecified) information model is

$$q(X_{i1}, X_{i2}, U_i) = \exp(X_{i1} - X_{i2} + U_i) / (1 + \exp(X_{i1} - X_{i2} + U_i)).$$

X_{i1}, X_{i2} and U_i are independently distributed: $X_{i1} \sim N(0, 1)$, $X_{i2} \sim N(0, 0.5)$, $U_i \sim N(0, 4)$.

In this scenario, doctors also process the full information (X_{i1}, X_{i2}, U_i) using an incorrect propensity score model. While the ROC curve corresponding to the predicted doctor model $q(X_{i1}, X_{i2}) \equiv \mathbb{E}[\mathbf{1}(q(X_{i1}, X_{i2}, U_i) > c_0) | X_{i1}, X_{i2}]$ lies below the optimal ROC curve corresponding to the correct propensity score model $p(X_{i1}, X_{i2})$, it still lies above the ROC curve corresponding to the individual doctor misspecified information model $q(X_{i1}, X_{i2}, U_i)$ and the aggregate doctor FPR/TPR pair. Collective wisdom in this case leads to limited improvement over the misspecified information model.

The third scenario is pictured in Figure 11(c). The ground-truth propensity score model is $p(X_i) = \exp(X_i) / (1 + \exp(X_i))$ but the doctors’ incorrect information model is

$$q(X_i, U_i) = \exp(-X_i + U_i) / (1 + \exp(-X_i + U_i)),$$

where X_i and U_i are distributed as in the first scenario depicted in Figure 11(a). In this model, doctors’ information processing capacity is very limited. The predicted doctor model $q(X_i) = \mathbb{E}[\mathbf{1}(p(X_i, U_i) > c_0) | X_i]$ exacerbates the misspecification of the doctors’ private information propensity score model, and leads to a ROC curve that lies strictly below the ROC curve corresponding to the individual doctor misspecified propensity score model $q(X_i, U_i)$.

The analysis in Figure 11 shows that depending on the extent of misspecification of the doctors’ information model, the predicted doctor model that aggregates the information among doctors using the subset of observable features available to the machine learning algorithm might either reduce or exacerbate the misspecification in the propensity score model. The resulting

ROC curve of the predicted doctor model might lie above or below the ROC curve of the doctors' information model.

5.3 Replacement strategies initiated by doctors

For a given decision maker, recognizing that machine algorithms are more likely to be applicable in some candidate cases than in others is important for a replacement model to achieve human and machine complementarity. Formalizing such a general empirical replacement model is difficult because of the unknown diagnosing model employed by doctors in the data and because of our lack of knowledge of doctors' preferences for the machine algorithm. To illustrate these difficulties, we experiment with a set of simulations in which doctors decide when to employ machine learning algorithm.

In the simulation setup, each patient is associated with three independently generated normally distributed features X_1, X_2, U , where $X_1 \sim N(0, 0.5)$, $X_2 \sim N(0, 1.5)$ and $U \sim N(0, 1)$. The probability of each patient being ill is a logit function of the features:

$$p(X_1, X_2, U) = e^{X_1 + X_2 + U} / (1 + e^{X_1 + X_2 + U}).$$

The labels are generated according to the probability model $p(X_1, X_2, U)$ for 30,000 patient cases. The diagnosis of doctors is modeled as a mixture between two decision rules. The first rule employs the correct probability model $p(X_1, X_2, U)$. The second rule replaces the probability model $p(x)$ by an uninformative uniformly distributed random variable $r \sim U(0, 1)$. The second rule applies to a situation where the occasional lack of medical knowledge by doctors results in randomized diagnosis. Specifically, we simulate doctor diagnosis \hat{Y} by

$$\hat{Y} = \begin{cases} \mathbb{1}(e^{X_1 + X_2 + U} / (1 + e^{X_1 + X_2 + U}) > c_d), & \text{if } X_1 \geq 0, \\ r > c_d, & \text{otherwise.} \end{cases}$$

In the above, $c_d = 0.5$ is the decision threshold for doctor diagnosis. The simulated dataset is divided into training, validation and test subsets by the ratio of 4:3:3. They are used to estimate model parameters, compute the ROC curve and calculate FPR/TPR pairs respectively. We first train a random forest model using features X_1 and X_2 , where U is interpreted as unobserved heterogeneity that is known to the doctors but not to the machine algorithm.

[Figure 12 about here.]

We simulate four replacement rules. They are illustrated in Figure 12. In the first rule, shown in Figure 12(a), doctors know when their medical knowledge is inadequate (e.g. when $X_1 < 0$) and choose to defer to the machine algorithm in such a situation. This method achieves complementarity between the human doctor and the machine algorithm. It produces

a FPR/TPR pair that is better than the Bayesian approach in which either all or none of the patients for each doctor are replaced. In the second rule, shown in Figure 12(b), doctors have partial but incomplete knowledge of when their medical knowledge is inadequate. Doctors defer to the machine algorithm when $X_1 < 0.5$. The second rule improves over the doctors, but does not outperform the Bayesian approach. Figure 12(c) use a replacement rule of $X_2 \leq -0.5$. In this case, the doctor does not know when they lack medical knowledge and the replacement reduces both FPR and TPR. In Figure 12(d), doctors mistakenly defer to the machine algorithm when they do have medical knowledge (e.g. when $X_1 \geq 0$), but make their own decision when they are uninformed (e.g. when $X_1 < 0$). The resulting FPR/TPR pair is strictly dominated by the original doctor diagnosis.

6 Conclusion

In this paper, we propose statistical tests for replacing human decision makers with algorithms. Decision rules that robustly dominate diagnoses made by humans can be determined based on the machine ROC curves. We propose both a heuristic frequentist approach and an alternative Bayesian posterior loss function approaches. By replacing a subset of decision makers with algorithms, we can achieve higher quality decision making outcome. We experiment with the two approaches using a dataset of pre-pregnancy checkups, and find that the replacement of a subset of doctors using the Bayesian approach significantly improves the overall performance of risky pregnancy detection. Furthermore, our results indicate that doctors who practice only at township clinics are more likely to be replaced, while doctors who practice only at county hospitals are less likely to be replaced.

Our analysis shows that both stable preference and decision-making quality are important for comparing machine algorithm with human decision makers. While allowing the juniors to make potentially suboptimal decisions for their patients and learn from the results has the potential of increasing the pool of high quality seniors, this is a very delicate issue involving complex welfare tradeoff between current and future generations of patients. In panel datasets with rich dynamic information, human decision makers can engage in information updating and peer learning. Our current dataset is only cross-sectional. The eventual pregnancy outcomes are typically not available to doctors when they diagnose consecutive patient cases. Juniors might also benefit more generally from offline learning without having to make substantial and high stake decisions.

7 Acknowledgments

We thank the editors and two anonymous referees, Brendan Beare, Bo Honore, Xiaohong Chen, Ron Gallant, Bruce Hansen, Peter Hansen, Bentley MacLeod, Jack Porter, Adam Rosen,

Andres Santos, George Tauchen, Valentin Verdier, and participants at various seminars and conferences for insightful comments. We also thank Yichuan Zhang, Xin Lin and Zhonghao Huang for excellent research assistance. This study was approved by the National Health Commission. Informed consents were obtained from all the NFPC participants. We acknowledge funding support from the National Science Foundation (SES 1658950 to Han Hong), the National Science Fund for Distinguished Young Scholars of China (71325007 to Ke Tang), the State’s Key Project of Research and Development Plan (2016YFC1000307 to Jingyuan Wang) and the National Natural Science Foundation of China (61572059 to Jingyuan Wang).

References

- Adepoju, Ibukun-Oluwa Omolade, Bregje Joanna Antonia Albersen, Vincent De Brouwere, Jos van Roosmalen, and Marjolein Zweekhorst**, “mHealth for clinical decision-making in sub-Saharan Africa: a scoping review,” *JMIR mHealth and uHealth*, 2017, 5 (3), e7185.
- Alur, Rohan, Loren Laine, Darrick K. Li, Manish Raghavan, Devavrat Shah, and Dennis Shung**, “Auditing for Human Expertise,” 2023.
- Ardila, Diego, Atilla P Kiraly, Sujeeth Bharadwaj, Bokyung Choi, Joshua J Reichler, Lily Peng, Daniel Tse, Mozziyar Etemadi, Wenxing Ye, Greg Corrado et al.**, “End-to-end lung cancer screening with three-dimensional deep learning on low-dose chest computed tomography,” *Nature medicine*, 2019, 25 (6), 954–961.
- Ashar, Yoni K, Jessica R Andrews-Hanna, Sona Dimidjian, and Tor D Wager**, “Empathic care and distress: predictive brain markers and dissociable brain systems,” *Neuron*, 2017, 94 (6), 1263–1273.
- Athey, Susan and Guido W Imbens**, “Machine learning methods that economists should know about,” *Annual Review of Economics*, 2019, 11, 685–725.
- **and Stefan Wager**, “Policy learning with observational data,” *Econometrica*, 2021, 89 (1), 133–161.
- Baeza-Yates, Ricardo, Berthier Ribeiro-Neto et al.**, *Modern information retrieval*, Vol. 463, ACM press New York, 1999.
- Bansal, Gagan, Tongshuang Wu, Joyce Zhou, Raymond Fok, Besmira Nushi, Ece Kamar, Marco Tulio Ribeiro, and Daniel Weld**, “Does the whole exceed its parts? the effect of ai explanations on complementary team performance,” in “Proceedings of the 2021 CHI Conference on Human Factors in Computing Systems” 2021, pp. 1–16.
- Berg, Tobias, Valentin Burg, Ana Gombović, and Manju Puri**, “On the rise of fintechns: Credit scoring using digital footprints,” *The Review of Financial Studies*, 2020, 33 (7), 2845–2897.
- Berk, Richard**, “An impact assessment of machine learning risk forecasts on parole board decisions and recidivism,” *Journal of Experimental Criminology*, 2017, 13 (2), 193–216.
- **, Hoda Heidari, Shahin Jabbari, Michael Kearns, and Aaron Roth**, “Fairness in criminal justice risk assessments: The state of the art,” *Sociological Methods & Research*, 2021, 50 (1), 3–44.

- Breiman, Leo**, “Random forests,” *Machine learning*, 2001, *45* (1), 5–32.
- Brennan, Meghan, Sahil Puri, Tezcan Ozrazgat-Baslanti, Zheng Feng, Matthew Ruppert, Haleh Hashemighouchani, Petar Momcilovic, Xiaolin Li, Daisy Zhe Wang, and Azra Bihorac**, “Comparing clinical judgment with the MySurgeryRisk algorithm for preoperative risk assessment: a pilot usability study,” *Surgery*, 2019, *165* (5), 1035–1045.
- Bulathwela, Sahan, María Pérez-Ortiz, Catherine Holloway, and John Shawe-Taylor**, “Could AI democratise education? Socio-technical imaginaries of an edtech revolution,” *arXiv preprint arXiv:2112.02034*, 2021.
- Chalfin, Aaron, Oren Danieli, Andrew Hillis, Zubin Jelveh, Michael Luca, Jens Ludwig, and Sendhil Mullainathan**, “Productivity and selection of human capital with machine learning,” *American Economic Review*, 2016, *106* (5), 124–127.
- Chan, David C, Matthew Gentzkow, and Chuan Yu**, “Selection with variation in diagnostic skill: Evidence from radiologists,” *The Quarterly Journal of Economics*, 2022, *137* (2), 729–783.
- Chan, Stephanie, Vidhatha Reddy, Bridget Myers, Quinn Thibodeaux, Nicholas Brownstone, and Wilson Liao**, “Machine learning in dermatology: current applications, opportunities, and limitations,” *Dermatology and therapy*, 2020, *10*, 365–386.
- Currie, Janet and WB MacLeod**, “Diagnosing expertise: Human capital, decision making, and performance among physicians,” *Journal of labor economics*, 2017, *35* (1), 1–43.
- Daneshjou, Roxana, Kailas Vodrahalli, Roberto A Novoa, Melissa Jenkins, Weixin Liang, Veronica Rotemberg, Justin Ko, Susan M Swetter, Elizabeth E Bailey, Olivier Gevaert et al.**, “Disparities in dermatology AI performance on a diverse, curated clinical image set,” *Science advances*, 2022, *8* (31), eabq6147.
- Donahue, Kate, Alexandra Chouldechova, and Krishnaram Kenthapadi**, “Human-algorithm collaboration: Achieving complementarity and avoiding unfairness,” in “Proceedings of the 2022 ACM Conference on Fairness, Accountability, and Transparency” 2022, pp. 1639–1656.
- Dwyer, Dominic B, Peter Falkai, and Nikolaos Koutsouleris**, “Machine learning approaches for clinical psychology and psychiatry,” *Annual review of clinical psychology*, 2018, *14*, 91–118.
- Elliott, Graham and Robert P Lieli**, “Predicting binary outcomes,” *Journal of Econometrics*, 2013, *174* (1), 15–26.
- Erickson, Bradley J, Panagiotis Korfiatis, Zeynettin Akkus, and Timothy L Kline**, “Machine learning for medical imaging,” *Radiographics*, 2017, *37* (2), 505–515.
- Esteva, Andre, Brett Kuprel, Roberto A Novoa, Justin Ko, Susan M Swetter, Helen M Blau, and Sebastian Thrun**, “Dermatologist-level classification of skin cancer with deep neural networks,” *nature*, 2017, *542* (7639), 115–118.
- Eubanks, Virginia**, *Automating inequality: How high-tech tools profile, police, and punish the poor*, St. Martin’s Press, 2018.

- Fauw, Jeffrey De, Joseph R Ledsam, Bernardino Romera-Paredes, Stanislav Nikolov, Nenad Tomasev, Sam Blackwell, Harry Askham, Xavier Glorot, Brendan O’Donoghue, Daniel Visentin et al.**, “Clinically applicable deep learning for diagnosis and referral in retinal disease,” *Nature medicine*, 2018, *24* (9), 1342–1350.
- Fekadu, Rufael, Anteneh Getachew, Yishak Tadele, Nuredin Ali, and Israel Goytom**, “Machine Learning Models Evaluation and Feature Importance Analysis on NPL Dataset,” *arXiv preprint arXiv:2209.09638*, 2022.
- Feng, Kai and Han Hong**, “Statistical Inference of Optimal Allocations I: Regularities and their Implications,” *arXiv preprint arXiv:2403.18248*, 2024.
- , – , **Ke Tang, and Jingyuan Wang**, “Properties of ROC curves,” *Working paper*, 2022.
- Fuster, Andreas, Matthew Plosser, Philipp Schnabl, and James Vickery**, “The role of technology in mortgage lending,” *The Review of Financial Studies*, 2019, *32* (5), 1854–1899.
- , **Paul Goldsmith-Pinkham, Tarun Ramadorai, and Ansgar Walther**, “Predictably unequal? The effects of machine learning on credit markets,” *The Journal of Finance*, 2022, *77* (1), 5–47.
- Guo, Jonathan and Bin Li**, “The application of medical artificial intelligence technology in rural areas of developing countries,” *Health equity*, 2018, *2* (1), 174–181.
- Han, Seung Seog, Ilwoo Park, Sung Eun Chang, Woohyung Lim, Myoung Shin Kim, Gyeong Hun Park, Je Byeong Chae, Chang Hun Huh, and Jung-Im Na**, “Augmented intelligence dermatology: deep neural networks empower medical professionals in diagnosing skin cancer and predicting treatment options for 134 skin disorders,” *Journal of Investigative Dermatology*, 2020, *140* (9), 1753–1761.
- Hannun, Awni Y, Pranav Rajpurkar, Masoumeh Haghpanahi, Geoffrey H Tison, Codie Bourn, Mintu P Turakhia, and Andrew Y Ng**, “Cardiologist-level arrhythmia detection and classification in ambulatory electrocardiograms using a deep neural network,” *Nature medicine*, 2019, *25* (1), 65–69.
- Huang, Shih-Cheng, Anuj Pareek, Saeed Seyyedi, Imon Banerjee, and Matthew P Lungren**, “Fusion of medical imaging and electronic health records using deep learning: a systematic review and implementation guidelines,” *NPJ digital medicine*, 2020, *3* (1), 136.
- Jin, Weina, Mostafa Fatehi, Ru Guo, and Ghassan Hamarneh**, “Evaluating the clinical utility of artificial intelligence assistance and its explanation on the glioma grading task,” *Artificial Intelligence in Medicine*, 2024, *148*, 102751.
- Johnson, Erin M and M Marit Rehavi**, “Physicians treating physicians: information and incentives in childbirth,” *American Economic Journal: Economic Policy*, 2016, *8* (1), 115–141.
- Johnson, Kipp W, Jessica Torres Soto, Benjamin S Glicksberg, Khader Shameer, Riccardo Miotto, Mohsin Ali, Euan Ashley, and Joel T Dudley**, “Artificial intelligence in cardiology,” *Journal of the American College of Cardiology*, 2018, *71* (23), 2668–2679.
- Kahneman, Daniel and Gary Klein**, “Conditions for intuitive expertise: a failure to disagree,” *American psychologist*, 2009, *64* (6), 515.
- Kawaguchi, Kohei**, “When will workers follow an algorithm? A field experiment with a retail business,” *Management Science*, 2021, *67* (3), 1670–1695.

- Kermany, Daniel S, Michael Goldbaum, Wenjia Cai, Carolina CS Valentim, Huiying Liang, Sally L Baxter, Alex McKeown, Ge Yang, Xiaokang Wu, Fangbing Yan et al.**, “Identifying Medical Diagnoses and Treatable Diseases by Image-Based Deep Learning,” *Cell*, 2018, *172* (5), 1122–1131.
- Kitagawa, Toru and Aleksey Tetenov**, “Who should be treated? empirical welfare maximization methods for treatment choice,” *Econometrica*, 2018, *86* (2), 591–616.
- Kleinberg, Jon, Himabindu Lakkaraju, Jure Leskovec, Jens Ludwig, and Sendhil Mullainathan**, “Human decisions and machine predictions,” *The Quarterly Journal of Economics*, 2018, *133* (1), 237–293.
- Kotz, Samuel, Narayanaswamy Balakrishnan, and Norman L Johnson**, *Continuous multivariate distributions, Volume 1: Models and applications*, Vol. 334, John Wiley & Sons, 2019.
- Liang, Huiying, Brian Y. Tsui, Hao Ni, Carolina C. S. Valentim, Sally L. Baxter, Guangjian Liu, Wenjia Cai, Daniel S. Kermany, Xin Sun, Jiancong Chen et al.**, “Evaluation and accurate diagnoses of pediatric diseases using artificial intelligence,” *Nature Medicine*, 2019, *25* (3), 433–438.
- Long, Erping, Haotian Lin, Zhenzhen Liu, Xiaohang Wu, Liming Wang, Jiewei Jiang, Yingying An, Zhuoling Lin, Xiaoyan Li, Jingjing Chen et al.**, “An artificial intelligence platform for the multihospital collaborative management of congenital cataracts,” *Nature biomedical engineering*, 2017, *1* (2), 0024.
- Lopez, Carolina, Anja Sautmann, and Simone Schaner**, “The contribution of patients and providers to the overuse of prescription drugs,” Technical Report, National Bureau of Economic Research 2018.
- Manski, Charles F**, “Credible ecological inference for medical decisions with personalized risk assessment,” *Quantitative Economics*, 2018, *9* (2), 541–569.
- Mbakop, Eric and Max Tabord-Meehan**, “Model selection for treatment choice: Penalized welfare maximization,” *Econometrica*, 2021, *89* (2), 825–848.
- McKinney, Scott Mayer, Marcin Sieniek, Varun Godbole, Jonathan Godwin, Natasha Antropova, Hutan Ashrafian, Trevor Back, Mary Chesus, Greg S Corrado, Ara Darzi et al.**, “International evaluation of an AI system for breast cancer screening,” *Nature*, 2020, *577* (7788), 89–94.
- Mondal, Himel, Shaikat Mondal, and Rajeev K Singla**, “Artificial Intelligence in Rural Health in Developing Countries,” in “Artificial Intelligence in Medical Virology,” Springer, 2023, pp. 37–48.
- Mullainathan, Sendhil and Jann Spiess**, “Machine learning: an applied econometric approach,” *Journal of Economic Perspectives*, 2017, *31* (2), 87–106.
- **and Ziad Obermeyer**, “Diagnosing physician error: A machine learning approach to low-value health care,” *The Quarterly Journal of Economics*, 2022, *137* (2), 679–727.
- O’neil, Cathy**, *Weapons of math destruction: How big data increases inequality and threatens democracy*, Crown, 2017.

- Peng, Sui, Yihao Liu, Weiming Lv, Longzhong Liu, Qian Zhou, Hong Yang, Jie Ren, Guangjian Liu, Xiaodong Wang, Xuehua Zhang et al.**, “Deep learning-based artificial intelligence model to assist thyroid nodule diagnosis and management: a multicentre diagnostic study,” *The Lancet Digital Health*, 2021, 3 (4), e250–e259.
- Rajpurkar, Pranav, Awni Y Hannun, Masoumeh Haghpanahi, Codie Bourn, and Andrew Y Ng**, “Cardiologist-level arrhythmia detection with convolutional neural networks,” *arXiv preprint arXiv:1707.01836*, 2017.
- Rambachan, Ashesh and Jonathan Roth**, “Bias in, bias out? Evaluating the folk wisdom,” *arXiv preprint arXiv:1909.08518*, 2019.
- , **Jon Kleinberg, Jens Ludwig, and Sendhil Mullainathan**, “An economic perspective on algorithmic fairness,” in “AEA Papers and Proceedings,” Vol. 110 2020, pp. 91–95.
- Sadhwani, Apar, Kay Giesecke, and Justin Sirignano**, “Deep learning for mortgage risk,” *Journal of Financial Econometrics*, 2021, 19 (2), 313–368.
- Sajjadiani, Sima, Aaron J Sojourner, John D Kammeyer-Mueller, and Elton Mykerezzi**, “Using machine learning to translate applicant work history into predictors of performance and turnover.,” *Journal of Applied Psychology*, 2019, 104 (10), 1207.
- Studdert, David M, Michelle M Mello, William M Sage, Catherine M DesRoches, Jordon Peugh, Kinga Zapert, and Troyen A Brennan**, “Defensive medicine among high-risk specialist physicians in a volatile malpractice environment,” *Jama*, 2005, 293 (21), 2609–2617.
- Swanson, Kyle, Eric Wu, Angela Zhang, Ash A Alizadeh, and James Zou**, “From patterns to patients: Advances in clinical machine learning for cancer diagnosis, prognosis, and treatment,” *Cell*, 2023, 186 (8), 1772–1791.
- Tian, Fei, Dong Liu, Na Wei, Qianqian Fu, Lin Sun, Wei Liu, Xiaolong Sui, Kathryn Tian, Genevieve Nemeth, Jingyu Feng et al.**, “Prediction of tumor origin in cancers of unknown primary origin with cytology-based deep learning,” *Nature Medicine*, 2024, pp. 1–11.
- Trivedi, Anusua, Sumit Mukherjee, Edmund Tse, Anne Ewing, and Juan Lavista Ferres**, “Risks of using non-verified open data: A case study on using machine learning techniques for predicting pregnancy outcomes in india,” *arXiv preprint arXiv:1910.02136*, 2019.
- Uhm, Kwang-Hyun, Seung-Won Jung, Moon Hyung Choi, Hong-Kyu Shin, Jae-Ik Yoo, Se Won Oh, Jee Young Kim, Hyun Gi Kim, Young Joon Lee, Seo Yeon Youn et al.**, “Deep learning for end-to-end kidney cancer diagnosis on multi-phase abdominal computed tomography,” *NPJ precision oncology*, 2021, 5 (1), 54.
- Vallee, Boris and Yao Zeng**, “Marketplace lending: A new banking paradigm?,” *The Review of Financial Studies*, 2019, 32 (5), 1939–1982.
- Wang, Jingyuan, Edoardo Gallo, Wei Zhang, Ke Tang, and Han Hong**, “Diagnosing with the help of artificial intelligence,” 2023. Working paper.
- Wang, Ziyi, Lijia Wei, and Lian Xue**, “Overcoming Medical Overuse with AI Assistance: An Experimental Investigation,” *arXiv preprint arXiv:2405.10539*, 2024.

- Yang, Jiehua, Mingfei Xie, Canpei Hu, Osamah Alwalid, Yongchao Xu, Jia Liu, Teng Jin, Changde Li, Dandan Tu, Xiaowu Liu et al.**, “Deep learning for detecting cerebral aneurysms with CT angiography,” *Radiology*, 2021, *298* (1), 155–163.
- Yoon, Jeewoo, Chaewon Kang, Seungbae Kim, and Jinyoung Han**, “D-vlog: Multi-modal vlog dataset for depression detection,” in “Proceedings of the AAAI Conference on Artificial Intelligence,” Vol. 36 2022, pp. 12226–12234.
- Yu, Feiyang, Alex Moehring, Oishi Banerjee, Tobias Salz, Nikhil Agarwal, and Pranav Rajpurkar**, “Heterogeneity and predictors of the effects of AI assistance on radiologists,” *Nature Medicine*, 2024, *30* (3), 837–849.
- Zeng, Jiaming, Berk Ustun, and Cynthia Rudin**, “Interpretable classification models for recidivism prediction,” *Journal of the Royal Statistical Society. Series A (Statistics in Society)*, 2017, pp. 689–722.

Table 1: Predicted abnormal birth probabilities and FPR rank of doctors

	Linear Term Only		With Nonlinear Term			
	(1)	(2)	(3)	(4)	(5)	(6)
FPR rank	0.003 (0.20)	-0.000 (-0.01)	-0.105 (-1.71)	0.120 (0.86)	-0.072 (-0.95)	0.156 (0.91)
Rank ²			0.111 (1.69)	-0.456 (-1.32)	0.072 (0.89)	-0.493 (-1.16)
Rank ³				0.385 (1.61)		0.380 (1.28)
Constant	0.206 (21.79)	0.205 (18.28)	0.224 (17.95)	0.205 (14.33)	0.216 (14.44)	0.197 (11.33)
Number of doctors	584	367	584	584	367	367
R^2	0.0001	0.0000	0.0059	0.0107	0.0025	0.0071

Notes: The table shows regression results for the relation between doctors' preferences and their patients' risk levels. In the baseline linear regression, the dependent variable is the patient's predicted risk by a random forest algorithm. The explanatory variable is the FPR rank of the patient's doctor. Regression results including quadratic and cubic terms are reported in columns (3) to (6) in the table. There are 584 doctors diagnosing at least 300 patient cases, and 367 doctors diagnosing at least 500 patient cases. Standard errors in parentheses are clustered by doctors.

Table 2: Doctor performance summary by multiple diagnosis classes

Panel A: FPRs for different diagnosis classes							
min patient cases	num negative	FP1	FP2	FP3	FPR1	FPR2	FPR3
300	554195	51896	33266	20954	0.0934	0.0600	0.0524
500	470562	42636	27362	21233	0.0906	0.0581	0.0451
Panel B: TPRs for different diagnosis classes							
min patient cases	num positive	TP1	TP2	TP3	TPR1	TPR2	TPR3
300	29986	3250	1750	1941	0.108	0.0584	0.0647
500	24758	2589	1384	1412	0.104	0.0559	0.0570
Panel C: Precisions across diagnosis classes							
min patient cases	wife precision	husband precision		couple precision			
300	0.0589	0.0500		0.0626			
500	0.0572	0.0481		0.0624			

Notes: In the table, FPR1 denotes FPR where the label is abnormal birth and the diagnosis is wife being high risk; FPR2 and FPR3 are similarly defined for the diagnosis classes of husband being high risk and both spouses being high risk. Similarly for TPR1, TPR2 and TPR3.

Table 3: Characteristics of replaced doctors

	Panel A: Summary statistics by doctor type			
	num	log num	GDP	replacement ratio
county & town	276	6.797 (0.73)	3.956 (2.94)	0.522
county only	161	6.515 (0.65)	3.675 (2.27)	0.398
town only	43	6.409 (0.58)	3.038 (2.26)	0.512
	Panel B: Logistic regression		Panel C: TPR kernel regression	
	(1)	(2)	(3)	(4)
log num	0.896 (2.85)	0.885 (3.20)	0.000251 (0.04)	0.000117 (0.02)
GDP percap	-0.0114 (-0.37)	-0.0124 (-0.41)		0.000569 (0.28)
count only		-0.367 (-1.99)	0.0172 (2.04)	0.0181 (1.99)
town only		0.359 (0.86)	-0.0273 (-1.73)	-0.0235 (-1.63)
FPR			0.958 (44.02)	0.954 (51.70)
Observations	457	457	480	469

Notes: Panel A shows the summary statistics of doctors grouped by type of their facility. Panel B shows regression results of a logistic regression with province level fixed effect. Cluster robust t -statistics are reported in parentheses. A more direct analysis of doctors performance is provided by a kernel regression of TPR on FPR and other covariates reported in Panel C. As in Panel B t -statistics are given in parentheses.

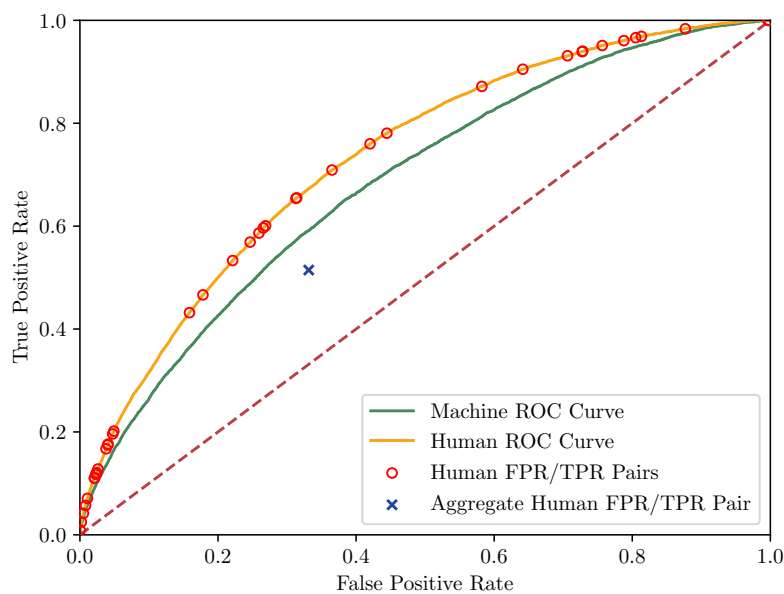


Figure 1: Individual and aggregate FPR/TPR pairs

Notes: When doctors use a correctly specified propensity score model to process both public and private information variables, the collection of FPR/TPR pairs for human decision makers, represented by the empty red circles, all lie above the green machine ROC curve. However, the aggregate FPR/TPR of human decision makers can still lie below the machine ROC curve. See section 2.5 for a more detailed discussion of how incentive heterogeneity can mask the nuances of comparing between machine learning and human decision making through an implication of Jensen’s inequality.

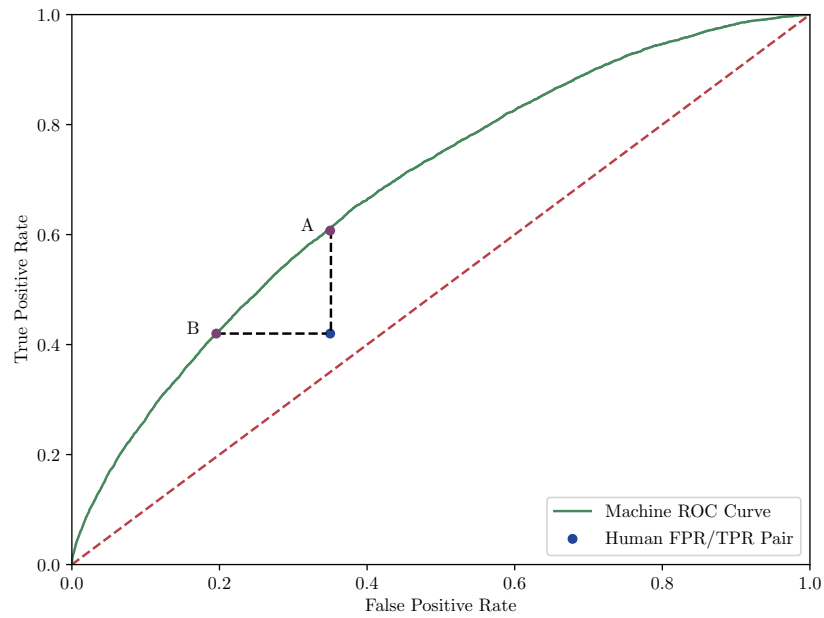


Figure 2: Population human FPR/TPR pair and the machine ROC curve

Notes: Point A matches the human FPR but has a higher TPR. Similarly, Point B matches the human TPR but has a lower FPR. The FPR and TPR of any point between points A and B on the machine ROC curve are smaller and larger, respectively, than the human decision maker's FPR/TPR pair.

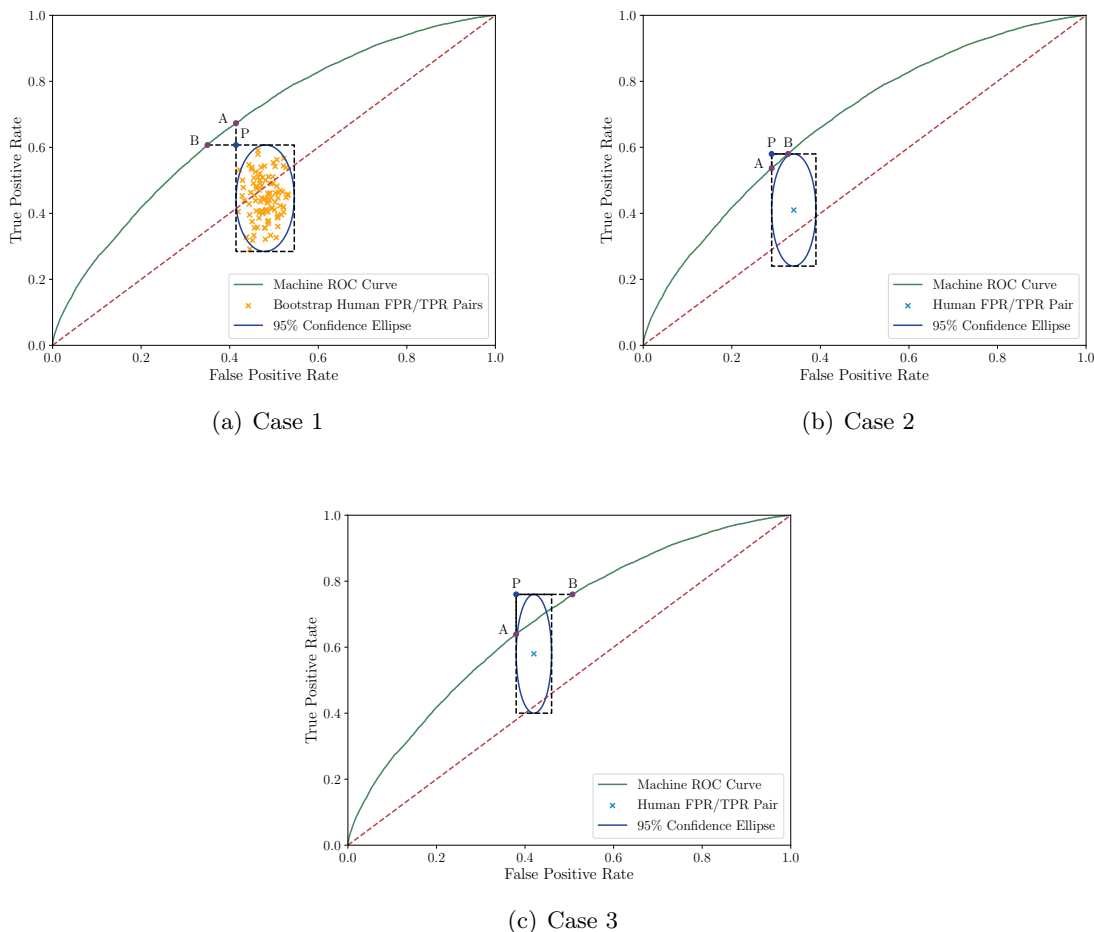
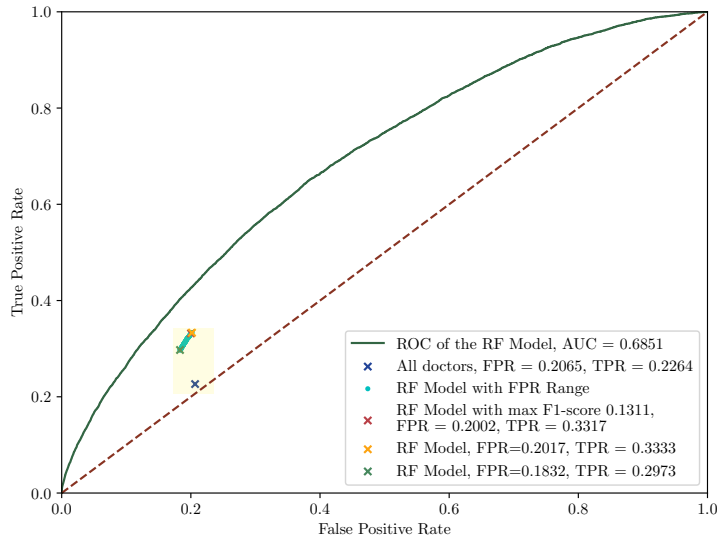
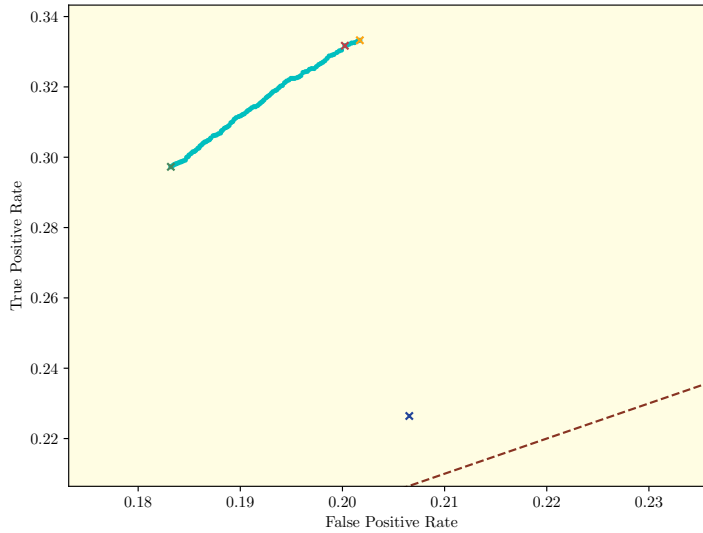


Figure 3: Three cases of the heuristic approach

Notes: The heuristic frequentist approach makes use of the point $P := (\alpha_{low}, \beta_{high})$ that corresponds to the smallest FPR and the highest TPR of the elliptical confidence set. Panel (a) shows the case where P lies below the machine ROC curve and where there exist dominating points on the curve. The yellow points are the bootstrapped FPR/TPR pairs. Panel (b) shows the case where the confidence set lies below the machine ROC curve, but there is no dominating point on the curve. Panel (c) shows the case where a portion of the confidence set lies above the machine ROC curve.



(a) ROC curve and FPR/TPR pairs of doctors and machine decisions



(b) Zoomed-in view

Figure 4: Empirical results of combining doctors' and machine decisions using the heuristic frequentist approach (doctors' diagnoses ≥ 300).

Notes: Panel (a) displays the ROC curve of the Random Forest classifier and the blue point representing the FPR/TPR pair of all doctors in the test set. The cyan interval shows the aggregate FPR/TPR pairs of combining retained doctors and the machine algorithm using different cutoff threshold choices in the frequentist replacement strategy. Panel (b) provides a magnified view of the cyan interval.

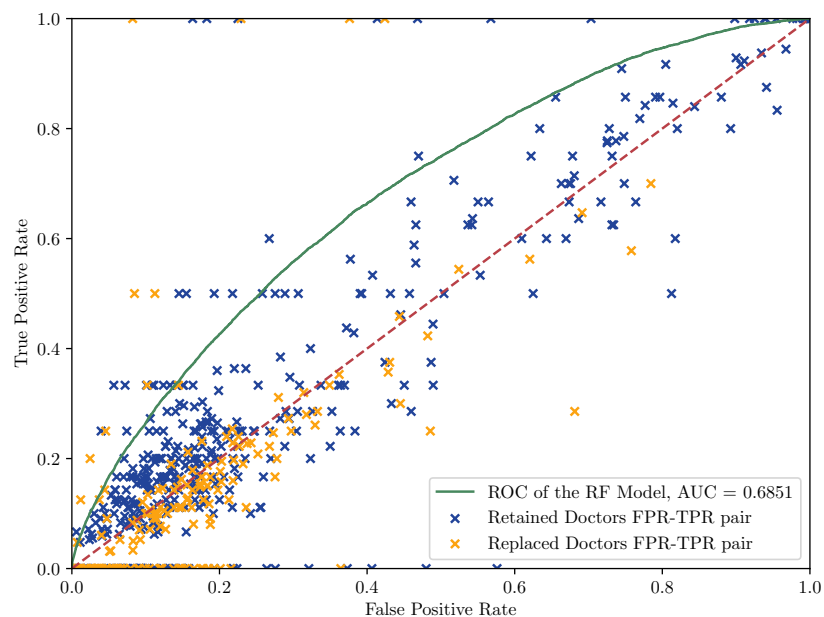
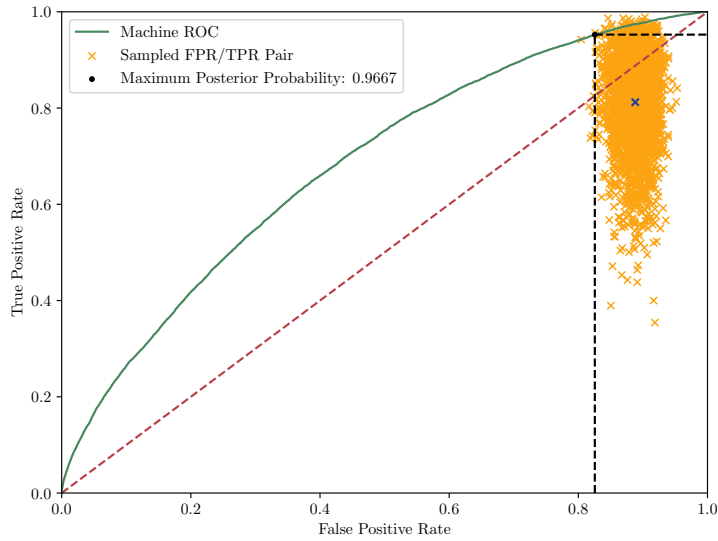
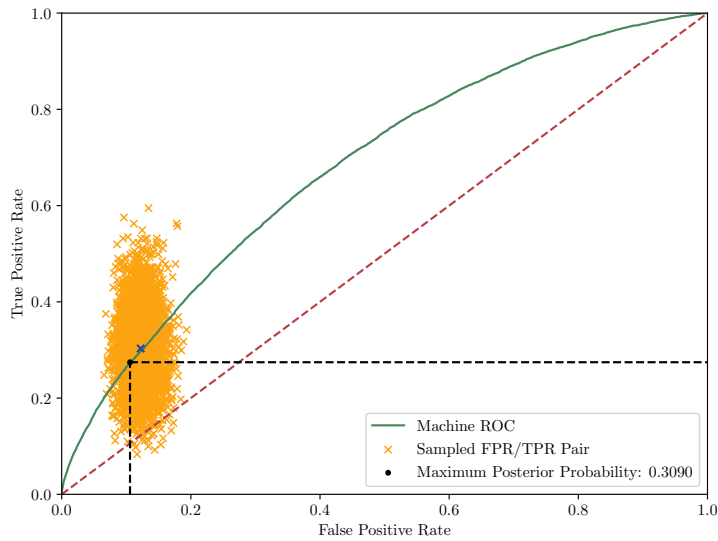


Figure 5: Scatter plot of replaced and retained doctors in the test dataset using the frequentist approach (doctors' diagnoses ≥ 300)

Notes: The FPR/TPR pairs in the scatter plot are calculated in the test dataset of patient cases for each doctor. It is possible for the FPR/TPR pairs of some of the replaced doctors to lie above the machine ROC curve in the test dataset. Two points that are quite close to each other can be of different replacement status due to different numbers of patients treated.



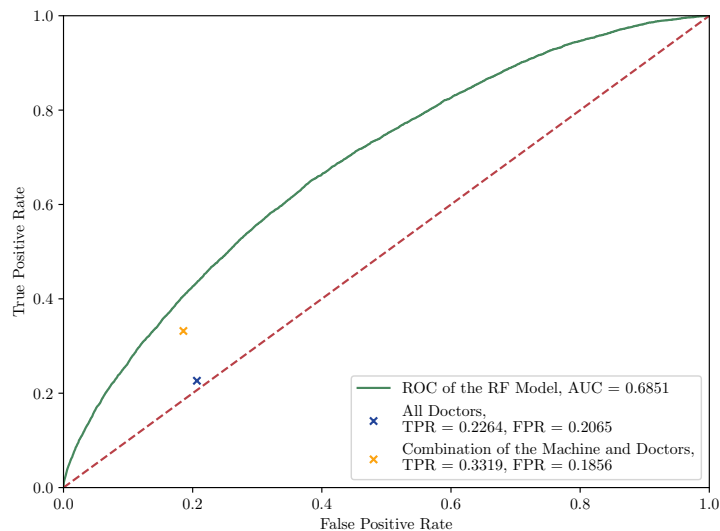
(a) The case where a doctor is replaced by the machine algorithm



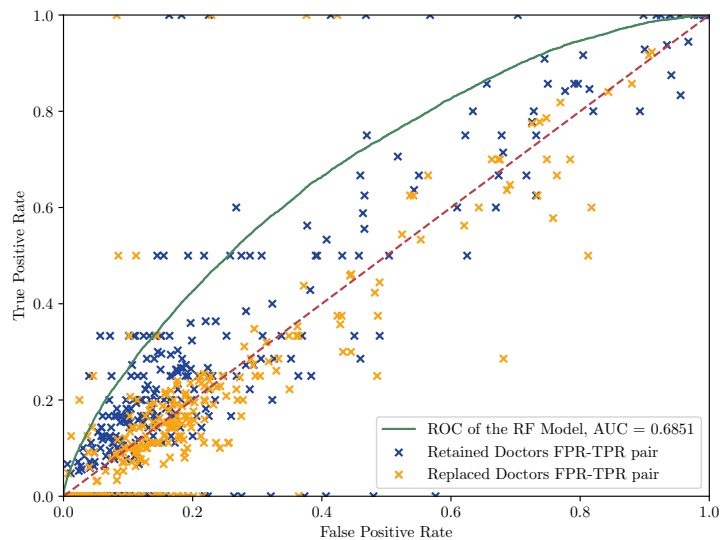
(b) The case where a doctor is not replaced by the machine algorithm

Figure 6: Illustration of replaced and retained doctors by the Bayesian approach

Notes: In the above two figures, the yellow points are sampled from the projection of the posterior Dirichlet distribution. One thousand draws are made for each panel. On the machine ROC curves, the black points are the points with the largest dominating posterior probability mass. Panel (a) shows a doctor whose posterior probability of being dominated is greater than 0.95. This doctor will be replaced by the machine decision rule corresponding to the black point. Panel (b) illustrates the opposite case where the doctor will not be replaced.



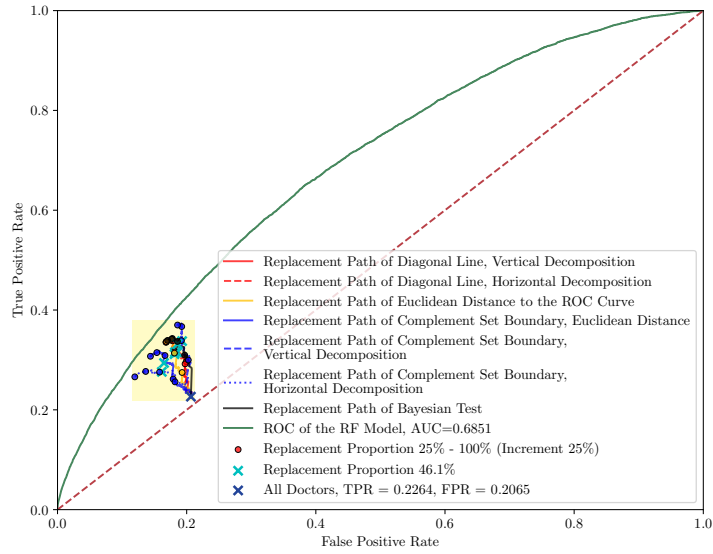
(a) ROC curve and FPR/TPR pairs of doctors and machine decisions



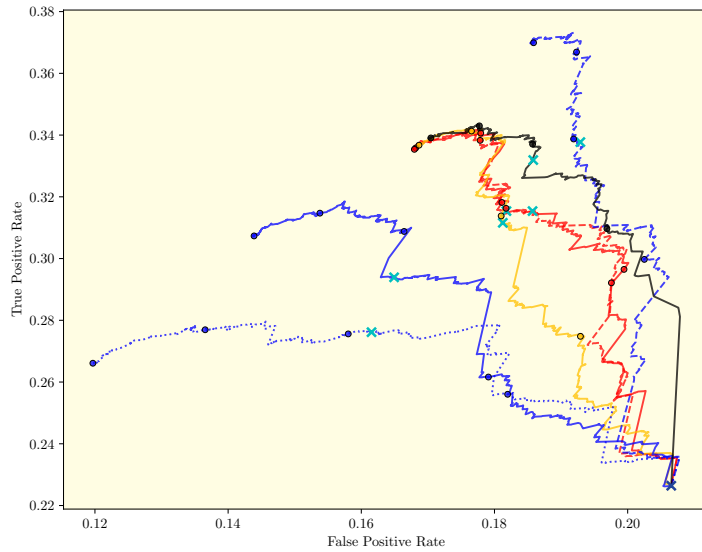
(b) Scatter plot of Bayesian doctor replacement in the performance dataset

Figure 7: Empirical results of the Bayesian approach (doctors' diagnoses ≥ 300).

Notes: The panel (a) draws the ROC curve in the test set of the Random Forest classifier, the FPR/TPR pair of all doctors, and the FPR/TPR pair of doctor/machine combination. The panel (b) scatterplot represents the FPR/TPR pairs of individual doctors, such that yellow points correspond to the replaced doctors and the blue points non-replaced doctors.



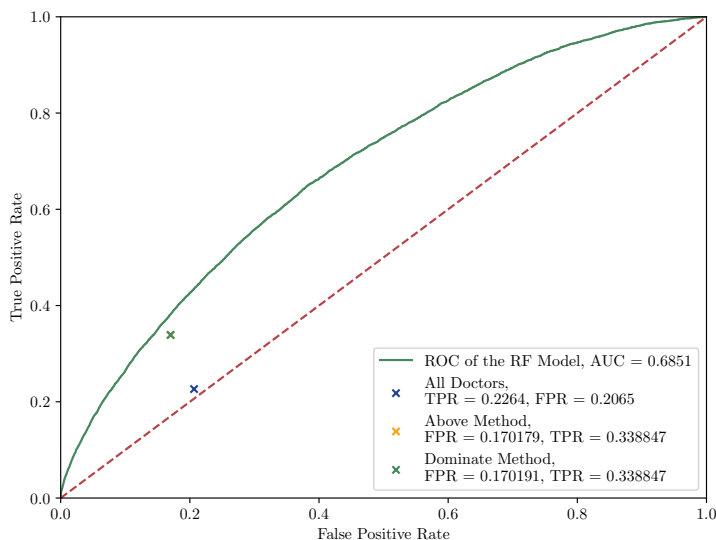
(a) ROC curve and replacement paths



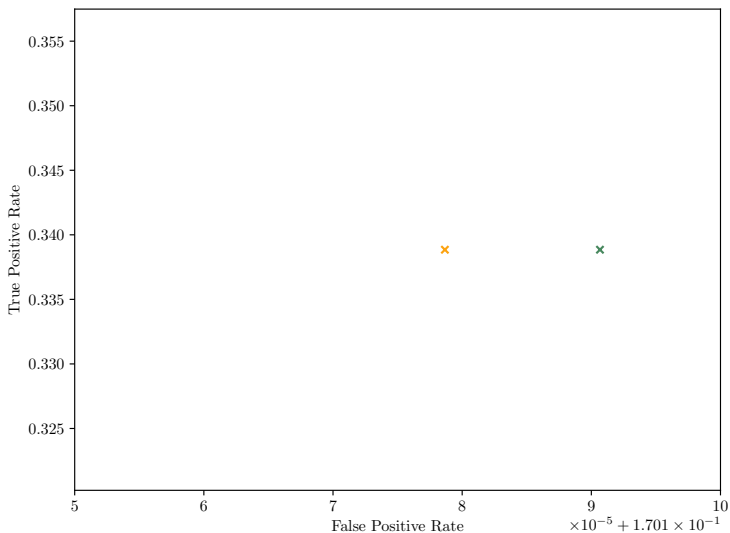
(b) Zoomed-in figure of replacement paths

Figure 8: Bayesian approach with loss functions constructed by Euclidean distance and randomized decomposition (doctors' diagnoses ≥ 300)

Notes: The replacement paths trace the dynamics of the aggregate FPR/TPR pairs of combining the doctor decisions with the machine decisions, when the replacement ratio increases from 0% of decisions entirely by human to 100% of decisions entirely by machine algorithms. Panel (b) magnifies a portion of panel (a) containing the replacement paths.



(a) ROC curve and FPR/TPR pairs of Doctors and machine decisions



(b) Zoomed-in FPR/TPR pairs of replacement outcomes

Figure 9: Alternative Null Hypothesis of Machine Algorithm: doctors are replaced by default and are retained only with strong evidence.

Notes: In the “dominate method” cross point, a doctor is retained if there exists a point on the machine ROC curve that is dominated by at least 95% of the posterior distribution of $p(\theta_H|\mathbb{D})$. A mere 6 doctors are retained in this method. In the “above method” cross point, a doctor is only retained if the posterior probability of $p(\theta_H|\mathbb{D})$ above the machine ROC curve is more than 95%. Only 7 doctors are retained using this method. These two points are almost indistinguishable in panel (a). Their difference is very small as shown in (b).

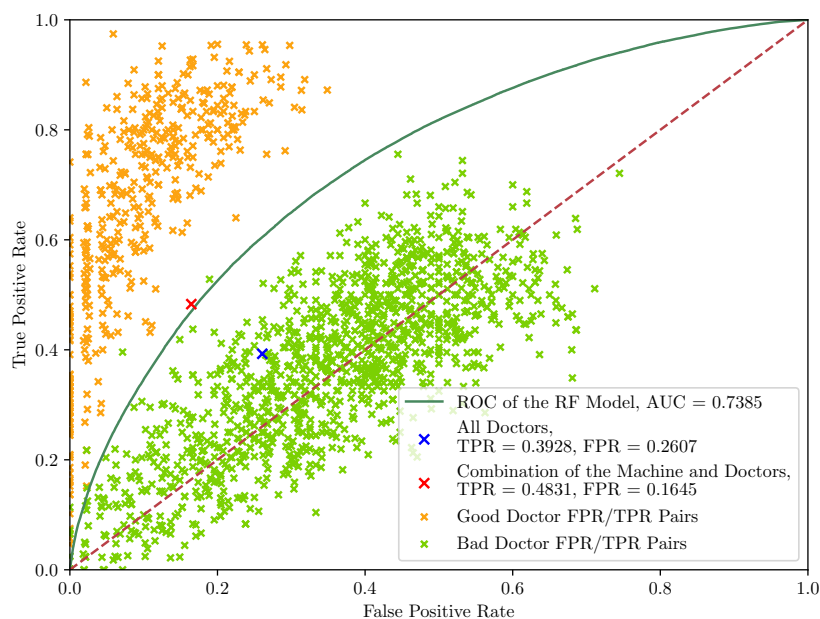
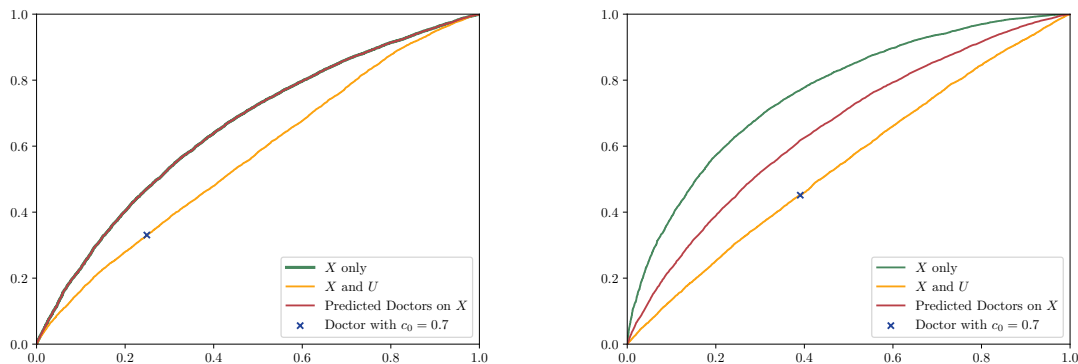


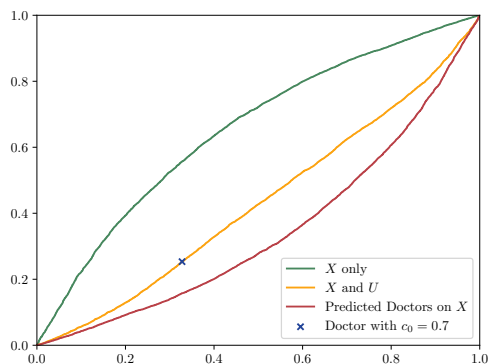
Figure 10: Synthetic data where combined FPR/TPR is above the machine ROC curve

Notes: In the figure, we simulate 750 doctors with better information than the machine algorithm and full information processing capabilities. These doctors are represented as the orange FPR/TPR points. Meanwhile, we simulate 1250 doctors with the same information but use misspecified prediction model in their decisions. These doctors are plotted as the green FPR/TPR points. Then we apply our Bayesian test approach to identify and replace the less capable doctors in the simulation. As shown in the figure, the doctor-algorithm combined aggregate FPR/TPR point lies above the machine ROC curve, an example of complementarity.



(a) Doctor using incorrect model based on private information: scenario 1

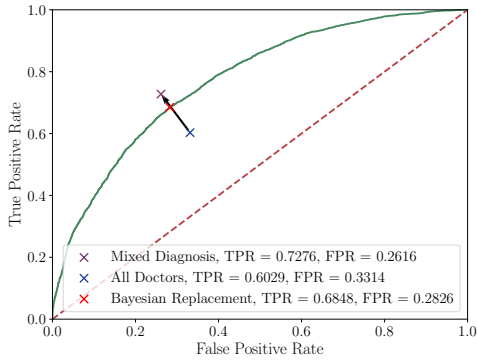
(b) Doctor using incorrect model based on private information: scenario 2



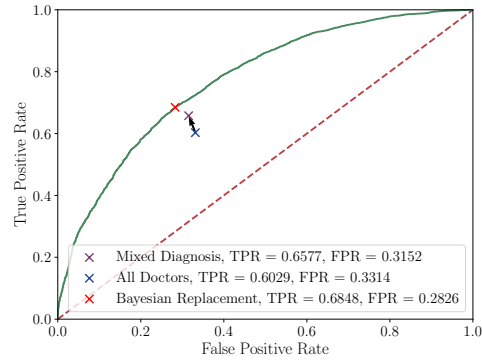
(c) Doctor using incorrect model based on private information: scenario 3

Figure 11: Three cases of learning from doctors

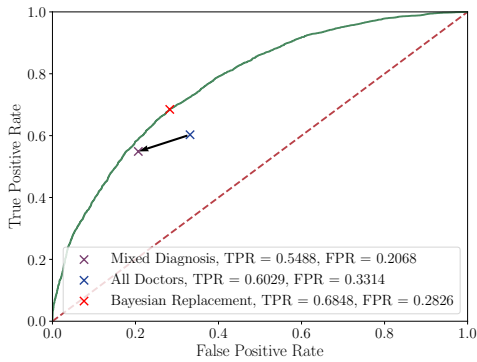
Notes: Instead of predicting ground-truth outcome, this figure illustrates three synthetic data examples where machine algorithms are applied to predict doctor’s diagnoses. Panel 11(a) shows a scenario where the machine algorithm improves upon the individual doctor diagnoses and generates the same ROC curve as a correctly specified model. Panel 11(b) shows a scenario where aggregating information from doctor diagnoses is beneficial but not sufficient to recover the optimal ROC curve. The last case is shown in Panel 11(c) where aggregating information from doctor diagnoses results in a ROC curve inferior to that of the misspecified prediction model.



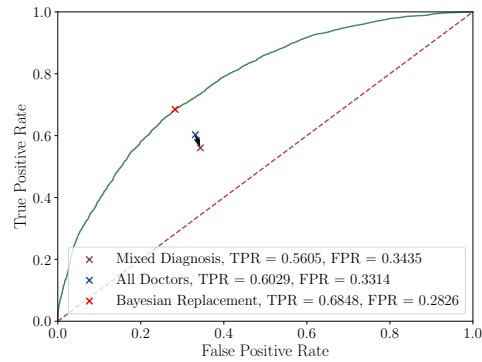
(a) Doctors well informed about themselves



(b) Doctors informed about themselves



(c) Doctors not informed about themselves



(d) Doctors misinformed about themselves

Figure 12: Replacement result under different replacement rules

Notes: A flexible replacing model allowing doctors to choose whether to apply the algorithm's decision has the potential of achieving human-machine complementarity. While, in this figure, we show that the performance of this strategy highly depends on doctors' choices. If the doctors do not have a clear recognition of their information weakness, this strategy may not perform well.

A Appendix for manuscript

STATISTICAL TESTS FOR REPLACING HUMAN DECISION MAKERS WITH
ALGORITHMS

A.1 Additional Lemmas and Proofs

Lemma A.1. *Let $p(X, U) = \mathbb{P}(Y = 1|X, U)$ and $p(X) = \mathbb{P}(Y = 1|X)$ be two correctly specified propensity score functions. The ROC curve generated $p(X, U)$ lies above the ROC curve generated by $p(X)$. Specifically, assuming that $\mathbb{P}(p(X, U) = c) = 0$ for all c , then if the decision rules $\mathbb{1}(p(x) > c)$ and $\mathbb{1}(p(x, u) > c')$ both achieve FPR level α for $0 \leq c, c' \leq 1$ and*

$$\mathbb{P}\{\mathbb{1}(p(X) > c) \neq \mathbb{1}(p(X, U) > c')\} > 0,$$

then $\mathbb{1}(p(x, u) > c')$ achieves higher TPR than $\mathbb{1}(p(x) > c)$ does.

PROOF. If we denote the ROC curve generated by $p(x)$ as

$$\beta_x(\alpha) = f_x(\alpha) = \frac{\mathbb{E}[Y\mathbb{1}(p(X) > c)]}{p} \quad \text{where } c \text{ satisfies } \frac{\mathbb{E}[(1-Y)\mathbb{1}(p(X) > c)]}{1-p} = \alpha,$$

then it can also be written as the solution of a constrained maximization program:

$$\beta_x(\alpha) = f_x(\alpha) = \max_{\phi(\cdot)} \frac{\mathbb{E}Y\phi(X)}{p} \quad \text{such that } \frac{\mathbb{E}[(1-Y)\phi(X)]}{1-p} = \alpha \text{ and } 0 \leq \phi(x) \leq 1.$$

See e.g. [Feng et al. \(2022\)](#). Similarly we can denote the ROC curve generated by $p(x, u)$ as

$$\begin{aligned} \beta_{x,u}(\alpha) = f_{x,u}(\alpha) &= \max_{\phi(\cdot, \cdot)} \frac{\mathbb{E}Y\phi(X, U)}{p} \\ \text{such that } &\frac{\mathbb{E}[(1-Y)\phi(X, U)]}{1-p} = \alpha \text{ and } 0 \leq \phi(x, u) \leq 1. \end{aligned}$$

Since the class of functions $\phi(x, u)$ includes the class $\phi(x, u) \equiv \phi(x)$ as a subset, it follows immediately that $\beta_{x,u}(\alpha) \geq \beta_x(\alpha)$. For the second part of our statement, consider the sets

$$\begin{aligned} S^+ &= \{(x, u) : \mathbb{1}(p(x, u) > c') > \mathbb{1}(p(x) > c)\}, \\ S^- &= \{(x, u) : \mathbb{1}(p(x, u) > c') < \mathbb{1}(p(x) > c)\}. \end{aligned}$$

By assumption, $\mathbb{P}(S^+ \cup S^-) > 0$. If $(x, u) \in S^+$, then $p(x, u) > c'$; if $(x, u) \in S^-$, then $p(x, u) \leq c'$. By assumption, $\mathbb{P}(p(X, U) = c') = 0$. Thus,

$$\iint [\mathbb{1}(p(x, u) > c') - \mathbb{1}(p(x) > c)] (p(x, u) - c') f_{X,U}(x, u) dxdu > 0.$$

The difference in power (TPR multiplied by p) then satisfies

$$\begin{aligned} & \int \int [\mathbf{1}(p(x, u) > c') - \mathbf{1}(p(x) > c)] p(x, u) f_{X,U}(x, u) dx du \\ & > c' \int \int [\mathbf{1}(p(x, u) > c') - \mathbf{1}(p(x) > c)] f_{X,U}(x, u) dx du \\ & = c' \int \int [\mathbf{1}(p(x, u) > c') - \mathbf{1}(p(x) > c)] p(x, u) f_{X,U}(x, u) dx du. \end{aligned}$$

The equality is due to the assumption that both decision rules achieve the same FPR:

$$\int \int [\mathbf{1}(p(x, u) > c') - \mathbf{1}(p(x) > c)] (1 - p(x, u)) f_{X,U}(x, u) dx du = 0.$$

We then have

$$\int \int [\mathbf{1}(p(x, u) > c') - \mathbf{1}(p(x) > c)] p(x, u) f(x, u) dx du > 0,$$

i.e., $\mathbf{1}(p(x, u) > c')$ achieves higher TPR. ■

Lemma A.2. *Consider a model where the human decision maker follows the classification rule $\hat{Y}_i = \mathbf{1}(p(X_i) > c(X_i, U_i))$ for the i th patient case, where $p(X_i)$ is a correctly specified propensity score function $p(X_i) = \mathbb{P}(Y_i = 1 | X_i)$ and U_i is a random variable that does not contain information about Y_i beyond those in X_i : $\mathbb{P}(Y_i = 1 | X_i, U_i) = \mathbb{P}(Y_i = 1 | X_i)$. Then the aggregate human decision maker FPR/TPR pair lies strictly below the ROC curve traced out by $\mathbf{1}(p(X_i) > c)$ when c varies between 0 and 1 under the following conditions:*

1. *The p -score $p(x)$ is uniformly bounded away from 0 and 1 on $x \in \mathcal{X}$, the support of X .*
2. *$p(X)$ is continuously distributed with a bounded and strictly positive density.*
3. *There is no $c \in [0, 1]$ such that $\mathbb{P}\{\mathbf{1}(p(X) > c) = \mathbf{1}(p(X) > c(X, U))\} = 1$.*

PROOF. First, we write human FPR/TPR pair as $\theta_H = (\alpha_H, \beta_H)$, where

$$\alpha_H = \frac{1}{1-p} \int \lambda(x) (1-p(x)) f_X(x) dx \quad \text{and} \quad \beta_H = \frac{1}{p} \int \lambda(x) p(x) f_X(x) dx.$$

In the above we have used $p = \mathbb{P}(Y_i = 1)$ and

$$\lambda(x) = \int \mathbf{1}(p(x) > c(x, u)) f_{U|X}(u|x) du.$$

We can then always find a threshold $c^* \in [0, 1]$ that satisfies

$$\alpha_O(c^*) = \frac{\int \mathbf{1}(p(x) > c^*) (1 - p(x)) f_X(x) dx}{1 - p} = \frac{\int \lambda(x) (1 - p(x)) f_X(x) dx}{1 - p} \equiv \alpha_H.$$

Given c^* , we then next define, on the ROC curve:

$$\beta_O(c^*) = \frac{\int \mathbf{1}(p(x) > c^*) p(x) f_X(x) dx}{p}.$$

By Neyman-Pearson arguments, $\phi^*(x) \equiv \mathbf{1}(p(x) > c^*)$ solves

$$\begin{aligned} & \max_{\phi(\cdot)} (1 - c^*) \int \phi(x) p(x) f_X(x) dx - c^* \int \phi(x) (1 - p(x)) f_X(x) dx \\ & = p(1 - c^*) \beta_O(c^*) - (1 - p) c^* \alpha_O(c^*) \geq p(1 - c^*) \beta_H - (1 - p) c^* \alpha_H. \end{aligned}$$

The difference between the two sides can be further written as

$$\begin{aligned} & p(1 - c^*) \beta_O(c^*) - (1 - p) c^* \alpha_O(c^*) - [p(1 - c^*) \beta_H - (1 - p) c^* \alpha_H] \\ & = \int (\mathbf{1}(p(x) > c^*) - \lambda(x)) (p(x) - c^*) f_X(x) dx, \end{aligned}$$

which is strictly positive unless $\mathbb{P}(\lambda(X) = \mathbf{1}(p(X) > c^*)) = 1$. This is ruled out by the stated assumptions. In particular, by condition 3, with positive probability, either one of the following two events (A and B) holds. In event A, $p(X) > c^*$ but $p(X) \leq c(X, U)$, in which case $\mathbf{1}(p(X) > c^*) = 1$ but $\lambda(X) < 1$. In event B, $p(X) \leq c^*$ but $p(X) > c(X, U)$, in which case $\mathbf{1}(p(X) > c^*) = 0$ but $\lambda(X) > 0$. Together $\mathbb{P}(\lambda(X) \neq \mathbf{1}(p(X) > c^*)) \geq \mathbb{P}(A \cup B) > 0$. ■

PROOF OF LEMMA 2.1. Recall the definitions of sample and population FPR/TPR pairs:

$$\hat{\alpha} = \frac{\sum_{i=1}^n (1 - Y_i) \hat{Y}_i}{\sum_{i=1}^n (1 - Y_i)}, \quad \hat{\beta} = \frac{\sum_{i=1}^n Y_i \hat{Y}_i}{\sum_{i=1}^n Y_i}, \quad \alpha = \frac{\mathbb{E}[(1 - Y_i) \hat{Y}_i]}{\mathbb{E}[1 - Y_i]}, \quad \beta = \frac{\mathbb{E}Y_i \hat{Y}_i}{\mathbb{E}Y_i}.$$

It follows from these definitions that for $\theta = (\alpha, \beta)'$ and $\hat{\theta} = (\hat{\alpha}, \hat{\beta})'$,

$$\sqrt{n}(\hat{\theta} - \theta) = \hat{H}^{-1} \frac{1}{\sqrt{n}} \sum_{i=1}^n \begin{pmatrix} (1 - Y_i) (\hat{Y}_i - \alpha) \\ Y_i (\hat{Y}_i - \beta) \end{pmatrix} \quad \text{where} \quad \hat{H} = \begin{pmatrix} 1 - \hat{p} & 0 \\ 0 & \hat{p} \end{pmatrix}.$$

By the Law of Large Numbers (LLN), \hat{H} converges to H in probability:

$$\hat{H} = H + o_{\mathbb{P}}(1) \quad \text{where} \quad H = \begin{pmatrix} 1 - p & 0 \\ 0 & p \end{pmatrix}.$$

By the multivariate central limit theorem (CLT),

$$\frac{1}{\sqrt{n}} \sum_{i=1}^n \begin{pmatrix} (1 - Y_i) (\hat{Y}_i - \alpha) \\ Y_i (\hat{Y}_i - \beta) \end{pmatrix} \xrightarrow{d} N(0, \Omega) \quad \text{where} \quad \Omega = \begin{pmatrix} \sigma_\alpha^2 & 0 \\ 0 & \sigma_\beta^2 \end{pmatrix}.$$

The relations $Y_i^2 = Y_i$, $(1 - Y_i)^2 = 1 - Y_i$ and $\hat{Y}_i^2 = \hat{Y}_i$ can be used to calculate that

$$\begin{aligned} \sigma_\alpha^2 &= \mathbb{E} \left[(1 - Y_i)^2 (\hat{Y}_i - \alpha)^2 = (1 - p) \alpha (1 - \alpha) \right], \\ \sigma_\beta^2 &= \mathbb{E} \left[Y_i^2 (\hat{Y}_i - \beta)^2 = p \beta (1 - \beta) \right]. \end{aligned}$$

It then follows from the multivariate Slutsky's Lemma that

$$\sqrt{n} (\hat{\theta} - \theta) \xrightarrow{d} N(0, \Sigma) \quad \text{where} \quad \Sigma = \begin{pmatrix} \frac{\alpha(1-\alpha)}{1-p} & 0 \\ 0 & \frac{\beta(1-\beta)}{p} \end{pmatrix}.$$

A typical concern with the application of central limit theorems is the quality of approximation in the finite sample when each of p , α and β is close to either 0 or 1. In particular, when the true population proportion of p is very close to either 0 or 1 relative to the sample size, both the numerator and the denominator in either $\hat{\alpha}$ or $\hat{\beta}$ may converge to a Poisson type limit random variable. Even in large samples, either $\hat{\alpha}$ or $\hat{\beta}$ remains random and may not converge to a population limit. In our application, the population parameter p is about 5%. Given that the sample size for each doctor is at least a few hundred, the asymptotic normal limit distribution still offers a reasonable approximation.

When either α or β is close to either 0 or 1, $\hat{\alpha}$ or $\hat{\beta}$ still converge to α or β , but their limit distributions and convergence rates can both be different. The normal approximation in the finite sample is likely to be more accurate for doctors whose FPR and TPR are bounded away from 0 and 1. While the frequentist and Bayesian approaches are not directly comparable, employing the Bayesian methodology does allow us to sidestep issues related to the asymptotic distribution approximation. ■

A.2 The Random Forest Algorithm

We implemented a random forest algorithm with N estimators and at most M features per node. For each node in a tree, no more than M features will be considered to obtain the best split. The algorithm works as follows:

1. For $i = 1$ to N :
 - (a) Draw a bootstrap sample $\tilde{\mathbb{D}}_i$ from the training data \mathbb{D} with replacements that has

the same sample size as \mathbb{D} .

- (b) Grow an unpruned tree T_i using $\tilde{\mathbb{D}}_i$ by repeating the following steps for each node of the tree until the nodes are pure or until the number of leaves for a node falls below the minimum number of samples required to split:
 - i. Randomly choose M features from the d dimensional input feature vector.
 - ii. Select the best of the M features to split using the Gini impurity criterion.
 - iii. Split the node into two subnodes using the best feature.
2. Obtain the output for the trees $\{T_i\}_{i=1}^N$.

Given an input feature vector \mathbf{x} , the random forest predicts the propensity score function by aggregating the results of N trees, where the class probability $m(\mathbf{x})$ is the average of the class probability of each tree in the forest.

A.3 Supplement to the Frequentist Approach

Frequentist approach machine decision thresholds: In sections 2.3 and 4.1, for each of the replaced doctors j , we generate the machine decision thresholds with a specific cutoff value c_j using the following algorithm. First, we find the largest ($c_{j,1}$) and smallest ($c_{j,N}$) cutoff thresholds corresponding to the end points of the dominating segment of the machine ROC curve, i.e., points B and A in Figure 3. To compute FPR/TPR pairs, we choose N cutoff thresholds along this dominating interval of the machine ROC curve between points B and A using the following procedure:

1. The stepsize of threshold spacing is set to $c_{j,\text{step}} = \frac{c_{j,N} - c_{j,1}}{N-1}$;
2. For each $l = 0, \dots, N-1$, the $l+1$ -th threshold between $c_{j,1}$ and $c_{j,N}$ is set to

$$c_{j,l+1} = c_{j,1} + lc_{j,\text{step}}.$$

For each $l = 1, \dots, N$, the l -th aggregate FPR/TPR pair is calculated using the decisions of all retained doctors and machine decisions based on $c_{j,l}$ for each replaced doctor.

A test between human FPR/TPR and machine ROC curve: An alternative is to test whether the population value of θ_H is above or below the machine ROC curve. The status quo of human decision making is typically chosen as the null hypothesis of $H_0 : \theta_H$ lies above ROC. This implies that a priori, *we maintain confidence in human decision making* unless overwhelming evidence suggests otherwise. As the machine ROC curve is represented by $\beta = g(\alpha)$, we can rewrite the null and alternative hypotheses as

$$H_0 : \beta_H \geq g(\alpha_H) \quad \text{against} \quad H_1 : \beta_H < g(\alpha_H).$$

Under the least favorable null hypothesis, the asymptotic distribution of a test statistic $\hat{t} = \hat{\beta}_H - g(\hat{\alpha}_H)$ follows from combining Lemma 2.1 with the Delta method. More precisely, if we define $\hat{B} = (-g'(\hat{\alpha}_H), 1)$, then the following central limit theorem holds under the least favorable null hypothesis:

$$\mathbb{P} \left(\frac{\sqrt{n} (\hat{\beta}_H - g(\hat{\alpha}_H))}{\sqrt{\hat{B} \hat{\Sigma} \hat{B}'}} \leq \Phi^{-1}(\alpha) \right) \rightarrow \alpha.$$

In the above, we use $\Phi^{-1}(\alpha)$ to denote the α -th percentile of the standard normal distribution. A test that rejects the null hypothesis when $\frac{\sqrt{n}(\hat{\beta}_H - g(\hat{\alpha}_H))}{\sqrt{\hat{B} \hat{\Sigma} \hat{B}'}}$ is less than $\Phi^{-1}(\alpha)$ will have asymptotic size α .

A.4 Robustness Analysis

To check the robustness of our approaches we also conduct the experiments based on doctors who diagnosed at least 500 patients. We have 367 such doctors and 495,320 patient cases in total. The classification set that is used to identify doctors contains 197,978 patient cases in the training sample and 148,579 patient cases in the validation sample. The remaining 148,763 cases are used to evaluate the performance of doctors and the algorithm. Other settings of the algorithm implementation are kept the same. We identify 135 doctors as replaced among 367 doctors. In other words, 36.8% of doctors are replaced by the algorithm and 63.2% of human doctors are retained in the performance data set.

Figure 13 shows the results of this experiment. Similar to Figure 4, the aggregate FPR/TPR pair of doctors on the performance set (the blue point) is 0.1942/0.2135. The AUC of the random forest model is 0.6892. The highest (yellow) point on the cyan interval has a FPR of 0.1947 and a TPR of 0.3419. These results represent an improvement of 60.1% in the TPR and a slight worsening of 0.3% in the FPR. The deterioration of the FPR is numerically possible because the FPR/TPR pairs are calculated out of sample using the performance data set.

[Figure 13 about here.]

The lower left (green) point of the cyan interval achieves 0.1719 for the FPR and 0.2965 for the TPR, representing an improvement of 38.9% in the TPR and a reduction of 11.3% in the FPR. The red point on the cyan curve achieves a maximum F1 score of 0.1353. The overall performance of experimenting with doctors diagnosing at least 500 patients does not differ substantially from the previous experiments with doctors diagnosing at least 300 patients. Figure 14 shows a scatter plot of the FPR/TPR pairs of both replaced and retained doctors against the ROC curve in the performance data set.

[Figure 14 about here.]

Figure 15(a) shows the experiment results for section 4.2 using only doctors who diagnosed at least 500 cases. Among all 367 such doctors, 201 are classified as replaced doctors. Therefore, 166 (45.2%) human doctors and 201 (54.8%) machine doctors are involved in the evaluation on the performance data set. The aggregate FPR and TPR for combined decision making are 0.1783 and 0.3292, respectively, representing an improvement of 54.2% on the TPR and a reduction of 8.2% on the FPR. Figure 15(b) is a scatter plot of the FPR/TPR pairs of both replaced and retained doctors against the ROC curve in the performance data set.

[Figure 15 about here.]

The replacement paths shown in the Figure 16, which correspond to the alternative loss functions in equations (12) to (15) and use only doctors who diagnosed at least 500 patient cases, are similar to Figure 8 for doctors diagnosing at least 300 cases.

[Figure 16 about here.]

A.5 Randomized Replacement by the Machine Algorithm

The experiments in section 4 identify doctors to be replaced by the machine algorithm. In this section we consider an extension where the machine decision is randomly accepted by the doctors according to a pre-specified probability. Each replaced doctor will accept the machine decision with a probability of $\lambda \in [0, 1]$ for each patient case. For each replaced doctor j , we generate decisions for their patient cases in the performance data set using the following randomized rule that combines $\hat{y}_{i,M}$ and $\hat{y}_{i,j}$ in Assumption 1:

$$\bar{Y}_{i,j} = \mathbf{1}(N_{i,j} \leq \lambda) \hat{Y}_{i,M} + \mathbf{1}(N_{i,j} > \lambda) \hat{Y}_{i,j},$$

where $N_{i,j}$ is independent and uniformly distributed on $[0, 1]$. The larger the λ , the more likely the doctor will accept the machine algorithm to make the decision.

Figure 17(a) shows the results of applying the randomized decision rule with different acceptance rates λ to the doctors diagnosing at least 300 patient cases identified by the Bayesian test in section 2.4.

[Figure 17 about here.]

The black crosses on the figures correspond to $\lambda \in \{0.2, 0.4, 0.6, 0.8\}$. As the acceptance rate λ grows, the black cross gradually moves from the blue cross (where all doctors make their own decisions; $\lambda = 0$) to the purple cross (where replaced doctors rely on machine decisions; $\lambda = 1$). The pairs of FPR/TPR under various levels of acceptance rates are tabulated in panel A of Table 4. The overall FPR/TPR performance improves monotonically when the replacement probability λ increases from 0 to 1.

[Table 4 about here.]

We also consider a setting where all doctors are randomized into being replaced by artificial intelligence. Figure 17(b) shows the results when different acceptance rates λ are used to randomize all doctors. When a patient case is randomized into being replaced by the machine learning, we continue to apply the baseline Bayesian test in (10) to determine the decision threshold on the machine ROC curve. Replacing identified doctors (45.2% of the total head-count) produces a much better FPR/TPR pair than randomly replacing the same proportion of doctors' decisions. In addition, replacing all doctors (the yellow cross) is not saliently better than replacing the identified doctors only (the purple cross).

Instead of relying on a single constant acceptance rate λ , patient cases can also be randomized by individualized acceptance rates λ 's that vary with the diagnosing doctor. We increase the acceptance probability λ when the posterior dominance probability \hat{q}_{\max} in the Bayesian test (10) goes up. Figure 18 displays two scenarios. In scenario 1, we rank the posterior dominance probability \hat{q}_{\max} of all doctors using the baseline Bayesian test (10) and assign them an acceptance rate λ that depends linearly on their ranks. The acceptance rate λ of the least dominated doctor, with rank 1, is set to 0, while λ for the most dominated doctor, with rank n , is set to 1. The acceptance probability for a doctor whose rank r is between 1 and n is $\lambda = \frac{r-1}{n-1}$. Scenario 2 is similar to scenario 1, but only the replaced doctors identified by the baseline Bayesian test (10) are randomized.

[Figure 18 about here.]

Figure 19 illustrates the consequence of an alternative procedure for determining the acceptance rates λ based on the reverse rank. Scenario 3 and scenario 4 are counterparts to scenarios 1 and 2. The difference is that here λ is calculated as $\frac{n-r}{n-1}$. We interpret the reverse rank ordering as retained doctors being more willing to accept machine decisions.

[Figure 19 about here.]

Compared with scenarios 1 and 2, the aggregate FPR/TPR pairs in scenario 3 and 4 are inferior. If replaced doctors are not willing to adopt the decision from a machine algorithm, the average diagnosis quality will not improve significantly. These results accord with our intuition. On the one hand, improving the overall FPR/TPR performance calls for higher acceptance rate for replaced doctors. On the other hand, using the machine algorithm to replace the retained doctors' decisions with high probability is less likely to be beneficial.

A.6 A patient-case specific substitution algorithm

There is a larger space for replacing a particular human decision maker only in specific contexts. In this appendix we experimented with an alternative decision making process during which

only some of the patient cases of a given doctor are diagnosed by the machine algorithm. Given that the diagnosis by the doctor is observed in each data point in addition to the outcome label, we use the machine algorithm not only to predict the likelihood of the outcome of abnormal birth, but also to evaluate when the doctor’s diagnosis are more likely to differ from the ground-truth outcome. The recognition that machine algorithms are more likely to be applicable in some candidate cases than in others for a given decision maker has been emphasized by [Donahue et al. \(2022\)](#), ? and ? among others.

The alternative substitution strategy we consider involves several steps. In the first step, we train a model, denoted as $F_{\text{mis}}(x)$, to predict the likelihood of a doctor misjudging a patient case. The label in this model is $\mathbb{1}(\hat{Y} \neq Y)$, where \hat{Y} is the diagnosis by the doctor whether this is a high risk pregnancy case and Y is the outcome of whether the observation corresponds to an abnormal birth. In the second step, we train another model, denoted as $F_{\text{doc}}(x)$, to predict the likelihood of a doctor diagnosing a patient case as high risk. In the third step, we use the patient cases for a given doctor to estimate the doctor’s ratio between the cost of false positive and the cost of false negative. The alternative substitution strategy combines information from these steps, and replaces a given patient case by the machine algorithm when the likelihood of the doctor’s diagnosis and the patient outcome being different is higher than a threshold. The threshold value depends on how likely a doctor will diagnose a patient case as high-risk. When the doctor’s cost of false positive is higher than the cost of false negative, the threshold should be lower when the doctor is more likely to diagnose a patient case as high-risk. Conversely, when the doctor’s cost of false positive is lower than the cost of false negative, the threshold should be higher when the doctor is more likely to diagnose a patient case as high-risk. Whether a doctor is likely to diagnose a patient case as high-risk is indicated by whether $F_{\text{doc}}(x)$ is higher than a given cut-off value.

Specifically, the replacement rule for a patient case with features x is given by

$$\begin{cases} F_{\text{mis}}(x) > c_r, & \text{if } F_{\text{doc}}(x) > c_d, \\ F_{\text{mis}}(x) > \frac{c_r}{t}, & \text{otherwise.} \end{cases}$$

In the above, t is the ratio between the cost of false negative and the cost of false positive for the given doctor. This ratio t is calculated as follows

$$t = (1 - \mathbb{P}(Y = 1)) / (s_t \cdot \mathbb{P}(Y = 1)), \tag{18}$$

where s_t is the slope of the tangent of the machine ROC curve at the point of the machine ROC curve which dominates the largest area of the simulated doctor’s posterior distribution as described in (10).

[Figure 20 about here.]

As illustrated in Figure 20, the slope of the aqua line tangent to ROC curve at the yellow cross is s_t . If C_{0R} denotes the false positive cost of misclassifying $y = 0$ as $y = 1$, and C_{1A} denotes the false negative cost of misclassifying $y = 1$ as $y = 0$, the expected cost of a decision rule is

$$\begin{aligned} & C_{0R}\mathbb{P}(Y = 0, \hat{Y} = 1) + C_{1A}\mathbb{P}(Y = 1, \hat{Y} = 0) \\ &= C_{0R}(1 - \mathbb{P}(Y = 1))\text{FPR} + C_{1A}\mathbb{P}(Y = 1)(1 - \text{TPR}) \\ &= C_{0R}(1 - \mathbb{P}(Y = 1))\text{FPR} - C_{1A}\mathbb{P}(Y = 1)\text{TPR} + C_{1A}\mathbb{P}(Y = 1). \end{aligned}$$

Therefore the slope of the tangent of the ROC curve at the optimizing pair of (FPR, TPR) that minimizes the expected cost is

$$s_t = \frac{C_{0R}(1 - \mathbb{P}(Y = 1))}{C_{1A}\mathbb{P}(Y = 1)},$$

implying that the ratio t is given by equation (18):

$$t = \frac{C_{1A}}{C_{0R}} = \frac{1 - \mathbb{P}(Y = 1)}{\mathbb{P}(Y = 1) s_t}.$$

Our second alternative substitution strategy is a variant of the first one. We train a model $F'_{\text{mis}}(x; \hat{Y})$ where the doctor's diagnosis enters directly into the feature set. The corresponding replacement rule for each patient case becomes

$$\begin{cases} F'_{\text{mis}}(x; \hat{Y}) > c_r, & \text{if } \hat{Y} = 1, \\ F'_{\text{mis}}(x; \hat{Y}) > \frac{c_r}{t}, & \text{otherwise.} \end{cases}$$

We experimented with the alternative substitution strategies on the set of doctors with at least 300 patient cases. First, we estimate F_{doc} , F_{mis} and F'_{mis} as three Random Forest models using data generating by the same sample splitting scheme as in the Bayesian test approach. Next we calculate the coefficient t in (18) for every doctor. The machine ROC is drawn using the validation set. Both $\mathbb{P}(Y = 1)$ and the Bayesian posterior distribution are evaluated on the combination of the training set and the validation set.

We set c_d to be 0.5 in the experiment, and find that the results are not sensitive to the choice of c_d . Then we calibrate the replacement threshold c_r for each doctor by equating the implied global replacement rate R to the Bayesian test approach. For the first alternative strategy, given the values of t and c_d , the global replacement rate R is related to each doctor's

c_r threshold by the following equation:

$$R = \mathbb{P}(F_{\text{mis}}(x) > c_r | F_{\text{doc}}(x) > c_d) \mathbb{P}(F_{\text{doc}}(x) > c_d) \\ + \mathbb{P}\left(F_{\text{mis}}(x) > \frac{c_r}{t} \middle| F_{\text{doc}}(x) \leq c_d\right) \mathbb{P}(F_{\text{doc}}(x) \leq c_d),$$

where the probabilities are estimated using the validation set.

Similarly, for the second alternative strategy, the threshold c_r is determined by equating

$$R = \mathbb{P}\left(F'_{\text{mis}}(x; \hat{Y}) > c_r | \hat{Y} = 1\right) \mathbb{P}(\hat{Y} = 1) \\ + \mathbb{P}\left(F'_{\text{mis}}(x; \hat{Y}) > \frac{c_r}{t} \middle| \hat{Y} = 0\right) \mathbb{P}(\hat{Y} = 0).$$

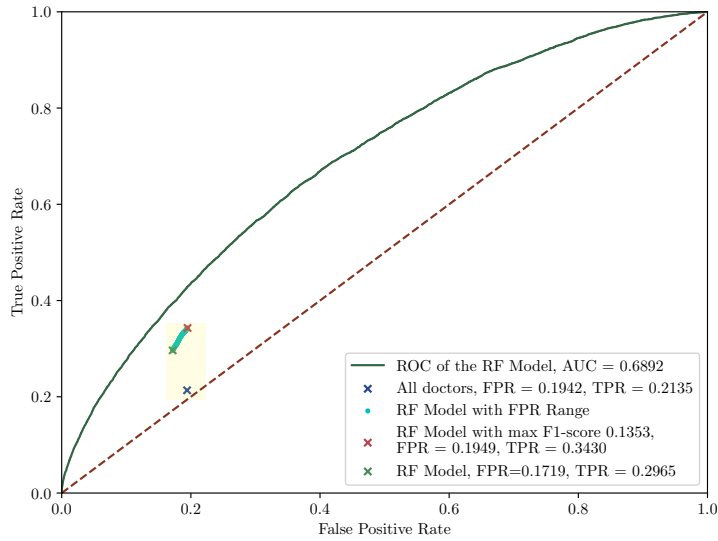
Finally, the test set is used to compute the FPRs and the TPRs from replacing a subset of each doctor's patient cases by the machine algorithm. The Bayesian test approach using 95% credible level replaces about 46% of the doctors and $R = 59.1\%$ of all patient cases. The experiment result is shown in Figure 21.

[Figure 21 about here.]

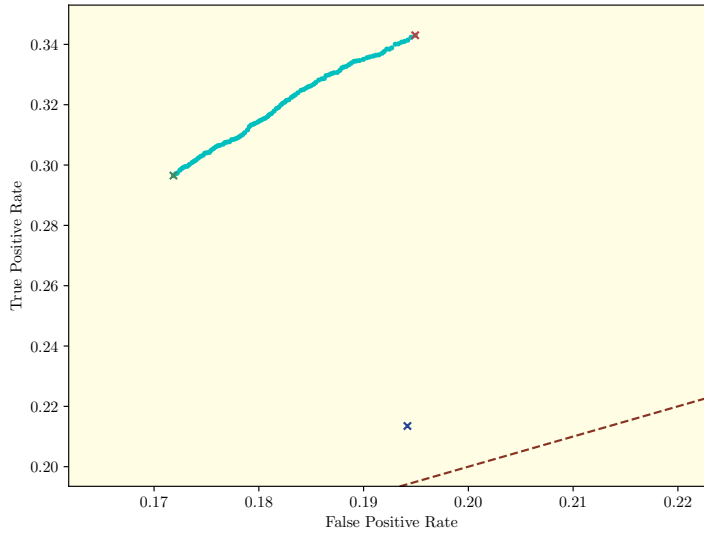
Table 4: Overall performance under different acceptance rates of machine decision

Panel A: Replaced doctors involved				
Accept Rate λ	FPR	Reduction of FPR	TPR	Improvement of TPR
0.0	0.2065	-	0.2264	-
0.2	0.2026	1.89%	0.2462	8.75%
0.4	0.1977	4.26%	0.2683	18.51%
0.6	0.1944	5.86%	0.2863	26.46%
0.8	0.1897	8.14%	0.3110	37.37%
1.0	0.1856	10.12%	0.3319	46.60%
Panel B: All doctors involved				
Accept Rate λ	FPR	Reduction of FPR	TPR	Improvement of TPR
0.0	0.2065	-	0.2264	-
0.2	0.1994	3.44%	0.2485	9.76%
0.4	0.1919	7.07%	0.2713	19.83%
0.6	0.1848	10.51%	0.2893	27.78%
0.8	0.1777	13.95%	0.3148	39.05%
1.0	0.1704	17.48%	0.3391	49.78%

Notes: Panel A tabulates the pairs of FPR/TPR under various levels of acceptance rates λ when the randomizeddecision is applied to the replaced doctors. Panel B includes all the doctors. The FPR/TPR pairs improves monotonically when the replacement probability λ increases from 0 to 1.



(a) ROC curve and FPR/TPR pairs of doctors and machine decisions



(b) Zoomed-in version

Figure 13: Empirical results of combining doctors' and machine decisions: the heuristic frequentist approach (doctors' diagnoses ≥ 500)

Notes: Panel (a) draws the ROC curve in the test set of the Random Forest classifier together with the blue point representing the FPR/TPR pair of all doctors. The cyan interval collects the FPR/TPR pairs of frequentist replacement strategies along the dominating segment of the machine ROC curve. Panel (b) provides a magnified view of the cyan interval.

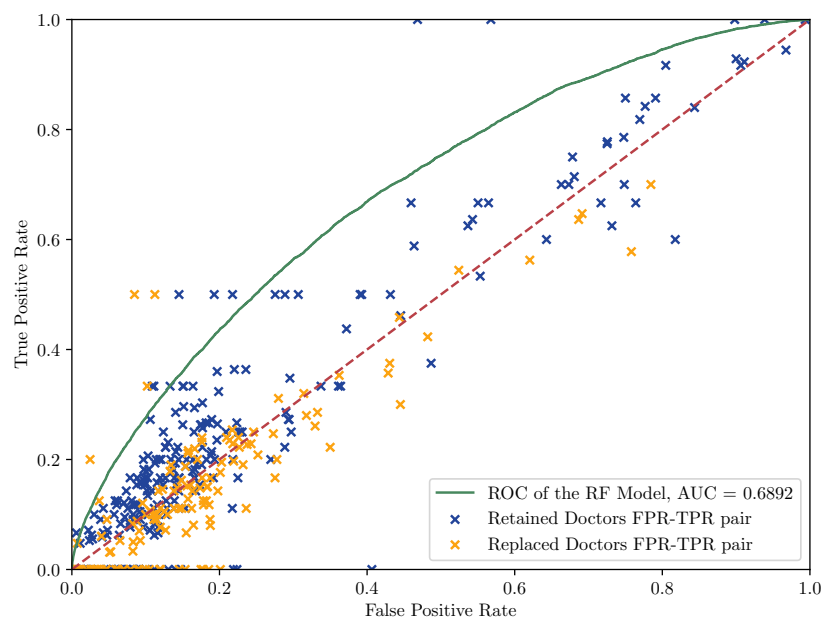
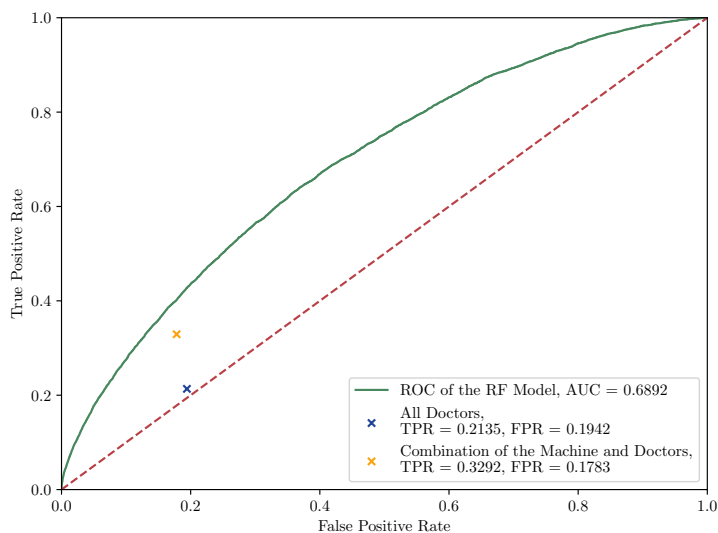
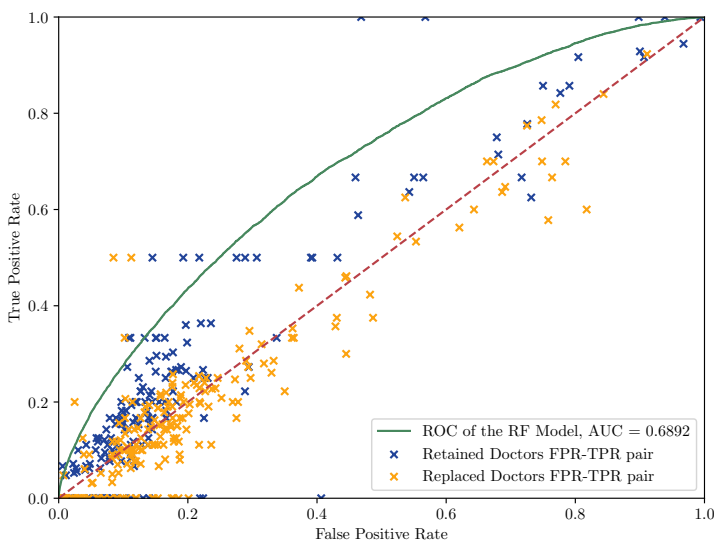


Figure 14: Scatter plot of frequentist doctor replacement in the performance data set (doctors' diagnoses ≥ 500)

Notes: The FPR/TPR pairs in the scatter plot are calculated in the test set of patient cases for each doctor using the raw data. It is possible for the TPR/FPR pairs of a small fraction of replaced doctor to lie above the machine ROC curve in the test set.



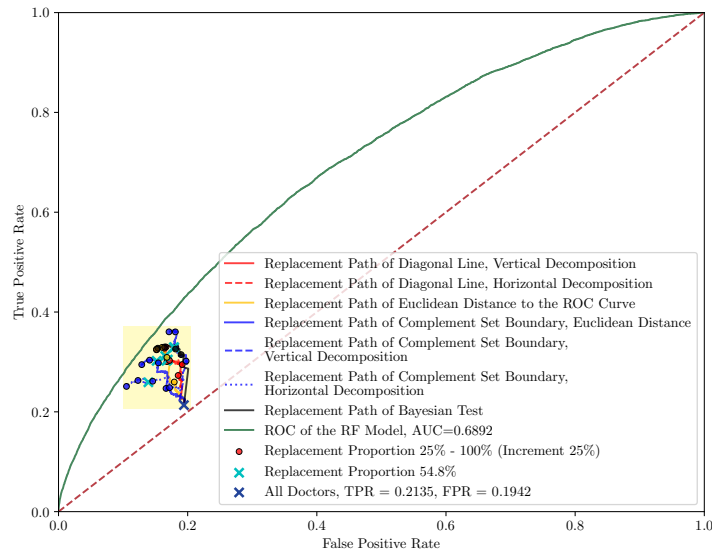
(a) ROC curve and FPR/TPR pairs of doctors and machine decisions



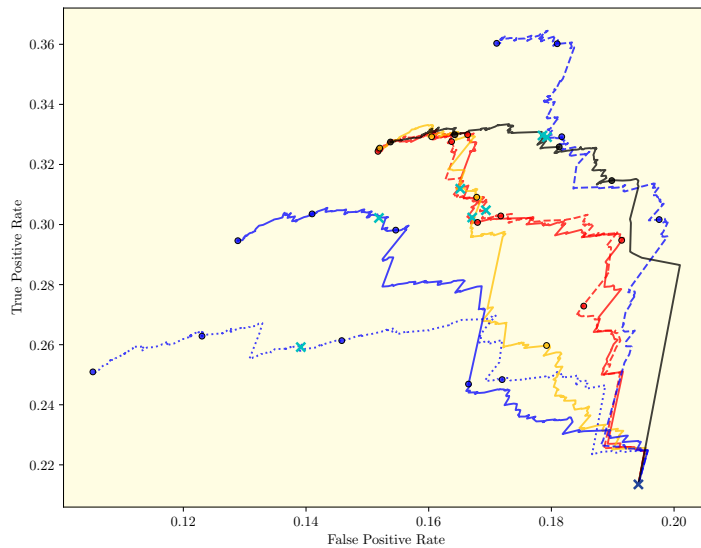
(b) Scatter plot of Bayesian doctor replacement in the performance data set

Figure 15: Empirical results of the Bayesian approach (doctors' diagnoses ≥ 500)

Notes: The panel (a) draws the ROC curve in the test set of the Random Forest classifier, the FPR/TPR pair of all doctors, and the FPR/TPR pair of doctor/machine combination. The panel (b) scatterplot represents the FPR/TPR pairs of individual doctors, such that yellow points correspond to the replaced doctors and the blue points non-replaced doctors.



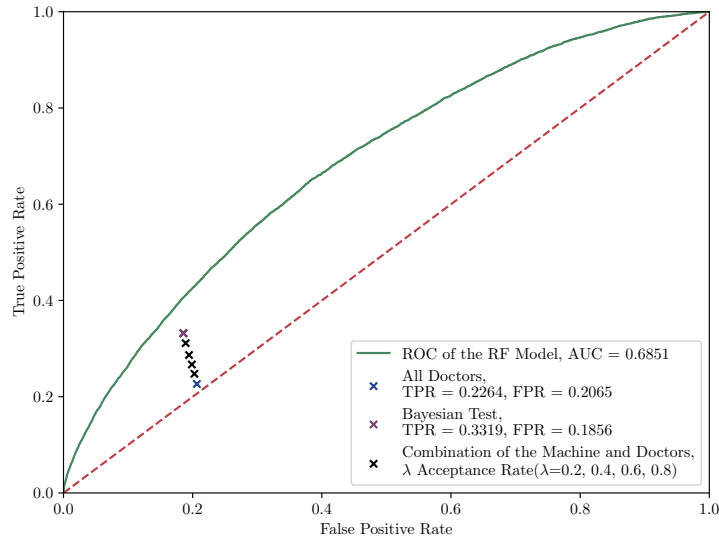
(a) ROC curve and Replacement Paths



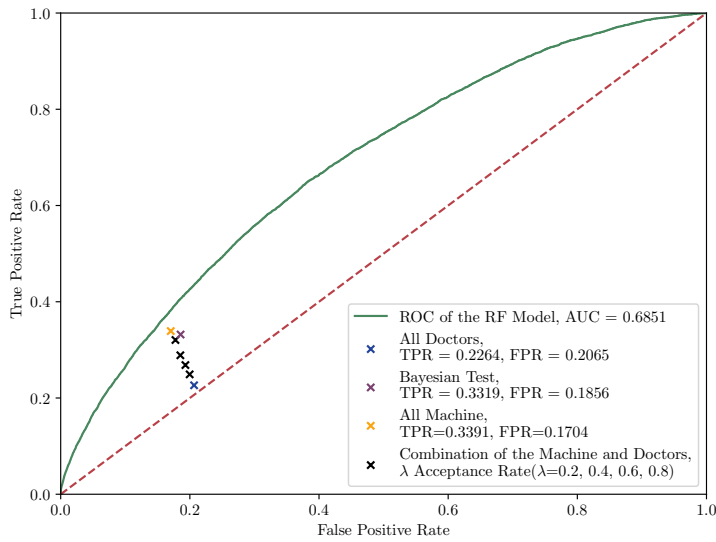
(b) Zoomed-in Figure of Replacement Paths

Figure 16: Bayesian Approach with Loss Functions Constructed by Euclidean Distance and Randomized Decomposition (Doctors' Diagnoses ≥ 500)

Notes: The replacement paths trace the dynamics of the aggregate FPR/TPR pairs of combining the doctor decisions with the machine decisions, when the replacement ratio increases from 0% of decisions entirely by human to 100% of decisions entirely by machine algorithms. Panel (b) magnifies a portion of panel (a) containing the replacement paths.



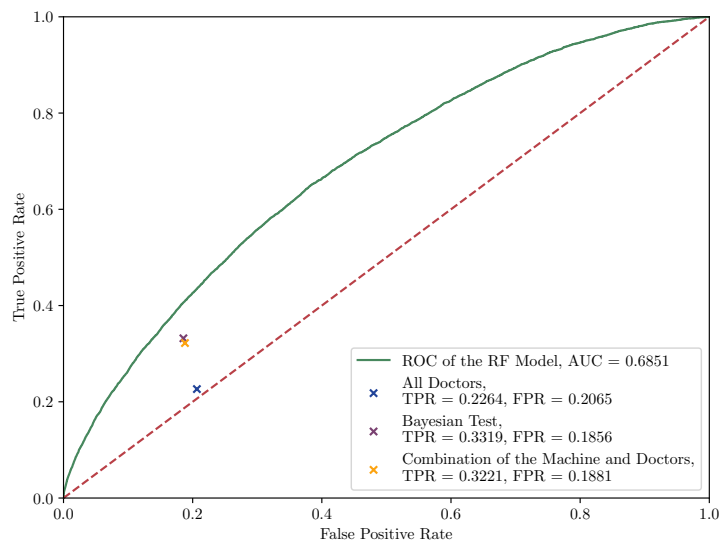
(a) Replaced doctors involved



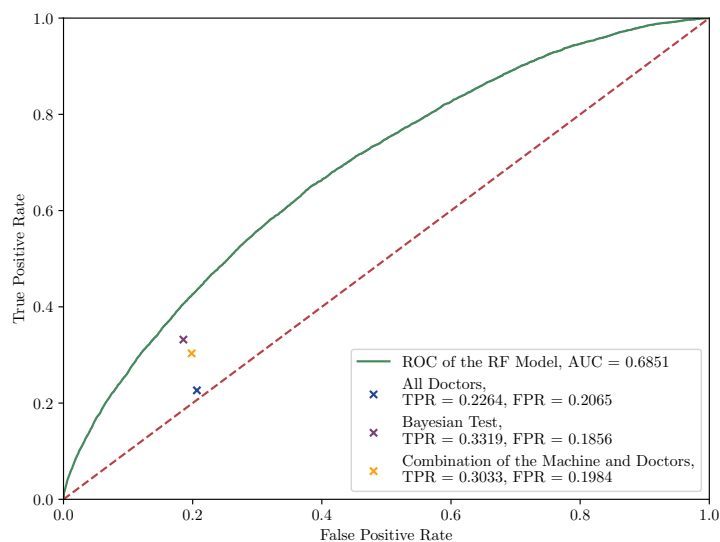
(b) All doctors involved

Figure 17: Results of the Bayesian approach under different acceptance rates

Notes: Figure (a) shows the results of applying the randomized decision rule with different acceptance rates λ to the replaced doctors diagnosing at least 300 patient cases. The FPR/TPR pairs are tabulated in Panel A of Table 4. Figure (b) includes all doctors as in Panel B of Table 4. Replacing all doctors only marginally improves upon the Bayesian test approach.



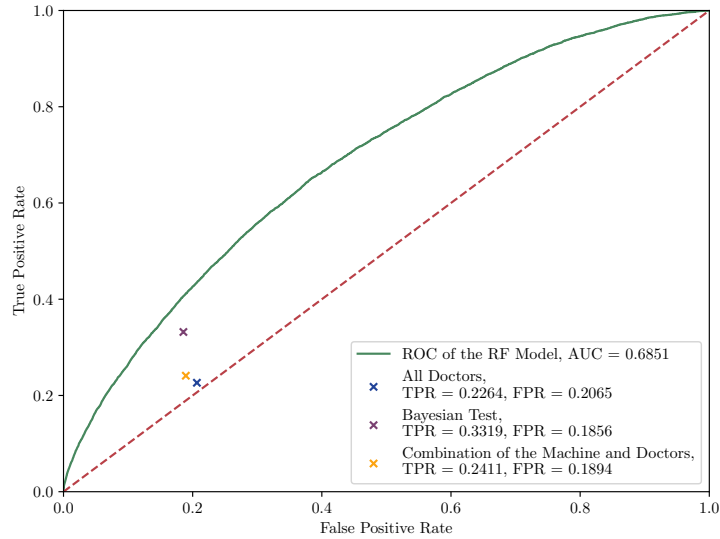
(a) Scenario 1: all doctors linear acceptance rate



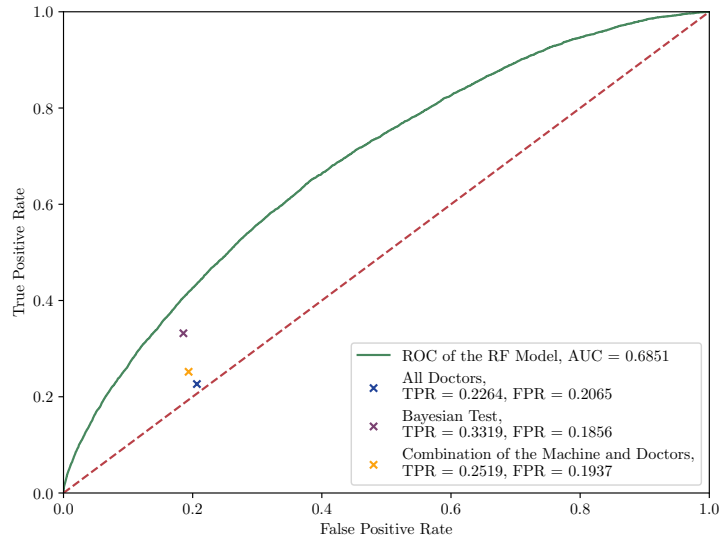
(b) Scenario 2: replaced doctors linear acceptance rate

Figure 18: Results of the Bayesian approach using capability dependence acceptance rates: replaced doctors more like to adopt the machine decisions

Notes: In this figure individualized acceptance rates specific to each doctors are used to randomize patient cases. Scenario 1 ranks the posterior dominance probability \hat{q}_{\max} of all doctors using the baseline Bayesian test (10) and assigns them an acceptance rate $\lambda = \frac{r-1}{n-1}$ that depends linearly on their ranks. Scenario 2 is similar to scenario 1, but only the replaced doctors identified by the baseline Bayesian test (10) are randomized.



(a) Scenario 3: all doctors involved



(b) Scenario 4: less capable involved

Figure 19: Results of the Bayesian approach using capability dependence acceptance rates: capable doctors more willing to accept the machine decisions

Notes: This figure shows the counterpart to Figure 18. The acceptance rate $\lambda = \frac{n-1}{n-1}$ depends on the reverse rank implying that retained doctors are more willing to accept machine decisions.

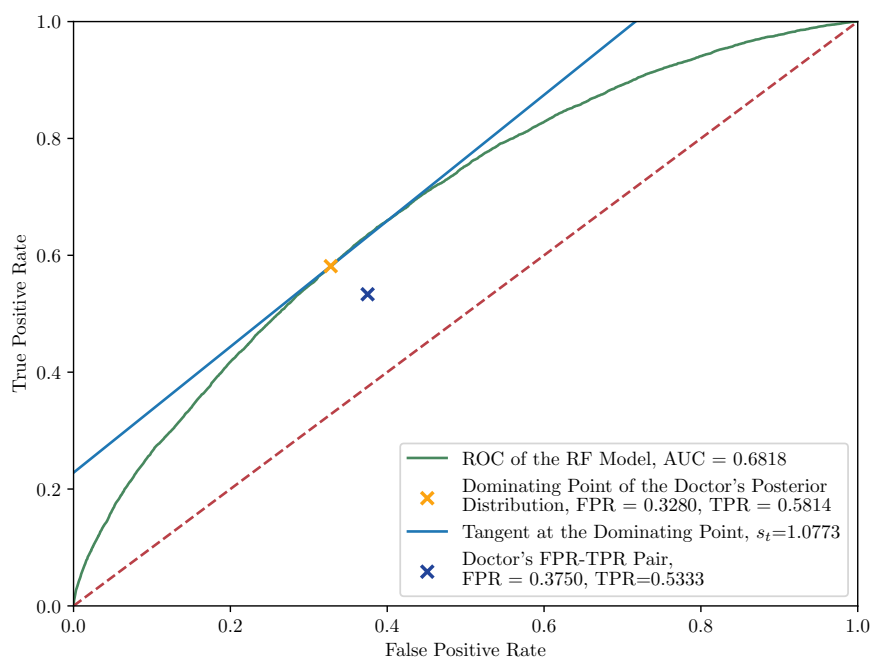
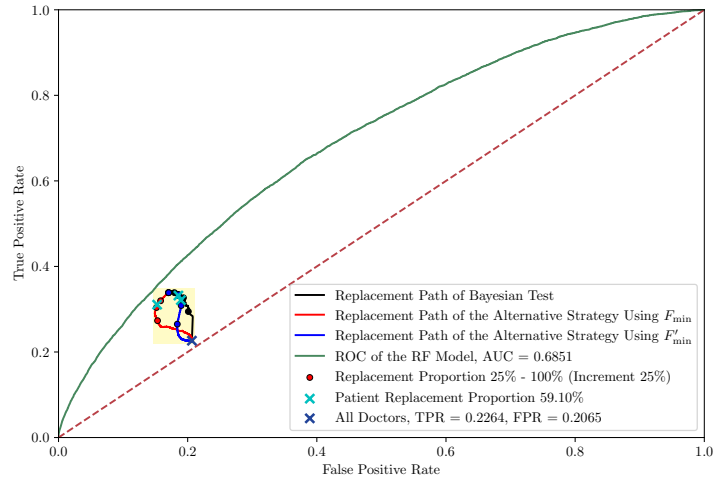
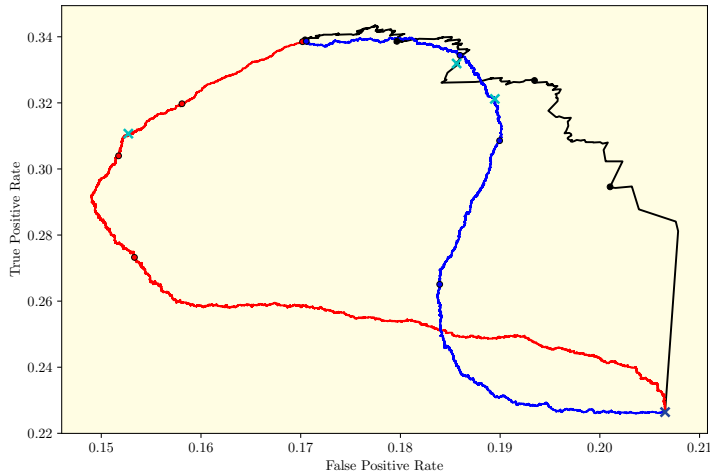


Figure 20: Calculation of ratio between the cost of false positive and the cost of false negative

Notes: This figure illustrates the calculation of the ratio between the cost of false negative and the cost of false positive for the given doctor in equation (18).



(a) ROC curve and replacement paths



(b) Zoomed-in version of replacement paths

Figure 21: The replacement paths of two alternative replacement approaches

Notes: Panel (b) plots the paths of FPR/TPR when the replacement rate R varies from 0 to 100%. While the replacement paths of the two alternative strategies are very different from the replacement path of the Bayesian test, none of the replacement paths dominate the others in FPR/TPR performance.